

Coherence length and penetration depth in strongly correlated superconductors

Niklas Witt^{1,2,*} Yusuke Nomura³ Sergey Brener¹ Ryotaro Arita^{4,5} Alexander I. Lichtenstein^{1,2} and Tim O. Wehling^{1,2,†}

¹*Institute of Theoretical Physics, University of Hamburg, Notkestraße 9-11, 22607 Hamburg, Germany*

²*The Hamburg Centre for Ultrafast Imaging, Luruper Chaussee 149, 22607 Hamburg, Germany*

³*Department of Applied Physics and Physico-Informatics,*

Keio University, 3-14-1 Hiyoshi, Kohoku-ku, Yokohama 223-8522, Japan

⁴*Research Center for Advanced Science and Technology,*

The University of Tokyo, 4-6-1 Komaba, Meguro-ku, Tokyo 153-8904, Japan

⁵*RIKEN Center for Emergent Matter Science (CEMS), 2-1 Hirosawa, Wako, Saitama 351-0198, Japan*

(Dated: April 4, 2025)

Superconductivity emerges from the spatial coherence of a macroscopic condensate characterized by two intrinsic length scales: the coherence length ξ_0 and the London penetration depth λ_L . While their description is well established in weak-coupling Bardeen-Cooper-Schrieffer (BCS) theory and Eliashberg theory, ξ_0 and λ_L are generally unknown quantities in strongly correlated superconductors. In this work, we establish a framework to calculate these length scales in microscopic theories and from first principles. Central to this idea are Nambu-Gor'kov Green functions under a constraint of finite-momentum pairing and their analysis with respect to the superconducting order parameter and resultant supercurrents. We illustrate with a multi-orbital model of alkali-doped fullerenes (A_3C_{60}) using Dynamical Mean-Field Theory (DMFT) how proximity of superconductivity, Jahn-Teller metallic, and Mott-localized states impact superconducting coherence, order parameter stiffness, and critical temperature. Our analysis reveals a “localized” superconducting regime with robustly short ξ_0 . Multi-orbital effects cause a domeless rise in the critical temperature as the pairing interaction is increased, setting this system apart from the BCS to Bose-Einstein-Condensate (BEC) crossover phenomenology.

The London penetration depth, λ_L , and the coherence length, ξ_0 , are two of the most fundamental characteristics of superconductors. They determine the critical surface spanned by critical magnetic fields, currents, and temperatures which a superconductor can tolerate. This makes them pivotal for the functionality of a wide range of superconducting applications [1, 2] spanning from electromagnets in magnetic resonance imaging [3–5] or particle accelerators [6, 7] to single-photon detectors [8, 9], SQUIDS [10, 11], superconducting diodes [12–14], or quantum computers [15].

Both intrinsic lengths, λ_L and ξ_0 , characterize different aspects of the superconducting (SC) condensate. The penetration depth is the length associated with the mass term that the vector potential gains through the *Anderson-Higgs* mechanism [16–18]. In consequence, magnetic fields decay exponentially over a distance λ_L inside a superconductor. λ_L is related to the SC stiffness which specifies the energy cost of spatial variations in the *phase* of the SC order parameter (OP). The coherence length, on the other hand, is the intrinsic length scale of OP amplitude variations and is associated with the *amplitude Higgs* mode. ξ_0 sets the scale below which amplitude and phase modes significantly couple such that spatial variations of the OP’s phase reduce its amplitude [18, 19].

Strongly correlated superconductors pose a platform

where fluctuation effects controlled by λ_L and ξ_0 play an important role, as is epitomized in the Uemura plot [20–25]. The interplay of λ_L and ξ_0 impacts critical temperatures [26, 27], it is relevant for the pseudogap formation [28–31] and the BCS-BEC crossover [25, 32–35], it influences magneto-thermal transport properties like the Nernst effect [24, 25, 36–39], and it might underlie the light-enhancement of superconductivity [40–47].

For weakly correlated superconductors, BCS theory and Eliashberg theory pose a well founded microscopic description of λ_L and ξ_0 [48–53]. Yet, in superconductors with strong electron correlations the validity of BCS or Eliashberg theory is unclear. To the best of our knowledge, ξ_0 is generally not known from theory in strongly correlated materials. Only approaches to determine λ_L exist where an approximate, microscopic assessment of the SC stiffness from locally exact theories has been established, albeit neglecting vertex corrections [54–59].

In this article, we present a microscopic approach to calculate λ_L and ξ_0 from the tolerance of SC pairing to spatial order parameter variations. Central to our approach are calculations in the superconducting state under a constraint of finite-momentum pairing (FMP). Via Nambu-Gor'kov Green functions we get direct access to the superconducting OP and depairing current j_{ap} which in turn yield ξ_0 and λ_L . The FMP constraint is the SC analog to planar spin spirals applied to magnetic systems [60–64]. As in magnetism, a generalized Bloch theorem holds [65] that allows us to consider FMP without supercells. As a result, our approach can be easily embedded in microscopic theories and *ab initio* approaches

* niklas.witt@physik.uni-hamburg.de

† tim.wehling@uni-hamburg.de

to tackle material-realistic calculations [56, 66–79].

Here, we implement FMP in Dynamical Mean-Field theory (DMFT) [74] to treat strongly correlated superconductivity. In DMFT, the interacting many-body problem is solved by self-consistently mapping the lattice model onto a local impurity problem. By this, local correlations are treated exactly. We apply the FMP constraint in DMFT to study a multi-orbital model inspired by alkali-doped fullerenes (A_3C_{60} with $A=K, Rb, Cs$) that has the peculiarity of an inverted Hund’s coupling $J < 0$. These materials host exotic s -wave superconductivity of critical temperatures up to $T_c \simeq 38$ K, being the highest temperatures among molecular superconductors [80–88], and they possibly demonstrate photo-induced SC at even higher temperatures [39, 44–46, 89, 90]. We find ξ_0 and λ_L in line with experiment for model parameter ranges derived for A_3C_{60} from *ab initio* estimates. For enhanced inverted Hund’s coupling, we reveal a previously hidden SC state that is characterized by “BEC-like” localized Cooper pairs with a minimal ξ_0 on the order of only 2–3 lattice constants, but with robust stiffness and high critical temperatures *without* a dome shape, in contrast to the usual BCS-BEC crossover.

I. SUPERCONDUCTIVITY WITH THE CONSTRAINT OF FINITE-MOMENTUM PAIRING.

The OP of a superconducting condensate with FMP has the form $\Psi_{\mathbf{q}}(\mathbf{r}) = |\Psi_{\mathbf{q}}|e^{i\mathbf{q}\mathbf{r}}$, where \mathbf{q} is the center-of-mass momentum of Cooper pairs [13, 91, 92]. FMP is well known from Fulde-Ferrel-Larkin-Ovchinnikov (FFLO) [92–95] theory, where the single-momentum phase used here corresponds to FF-type pairing. We contrast the OP for zero and finite momentum in real and momentum space in the top panel of Fig. 1. For FMP, the OP’s phase is a helix winding around the direction of \mathbf{q} , while the OP for zero momentum pairing is simply constant.

In the following, we explain how the introduction of FMP gives access to the characteristic SC length scales, ξ_0 and λ_L , through an analysis of momentum- and temperature-dependent OP and the closely connected charge supercurrent.

A. Ginzburg-Landau description

Before turning to the implementation in microscopic approaches, we motivate how the FMP constraint relates to λ_L and ξ_0 . The Ginzburg-Landau (GL) framework provides an intuitive picture to this connection which we summarize here and explain in detail in the Supplemental Material (SM) [65]. The GL low-order expansion of the free energy density f_{GL} in terms of the FMP-constrained

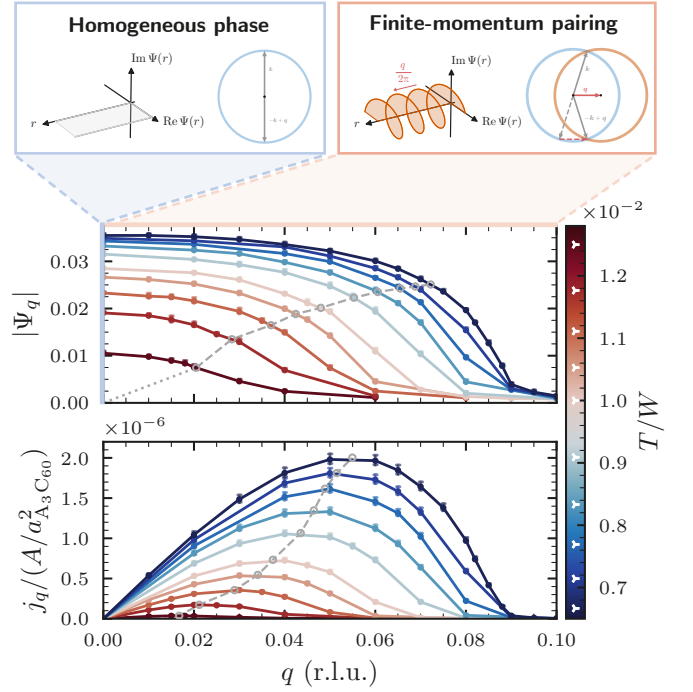


FIG. 1. Influence of finite-momentum pairing (FMP) constraint with momentum \mathbf{q} on superconducting condensate. Insets in the top panel sketch position and momentum space representation of the zero-momentum-pairing phase (left, $q = 0$) and the phase with finite-momentum pairing (right, $q > 0$) of the FMP order parameter (OP) $\Psi_{\mathbf{q}}(\mathbf{r}) = |\Psi_{\mathbf{q}}|e^{i\mathbf{q}\mathbf{r}}$. Bottom panels show the momentum dependence of the OP modulus and microscopic supercurrent $j_{\mathbf{q}}$ induced by the Cooper pair center-of-mass movement with $q = |\mathbf{q}|$ in reciprocal lattice units (r.l.u.). Gray lines indicate the points of extracting ξ and j_{dp} (see text). Shown data are results for the A_3C_{60} -inspired model (c.f. Eq. (7)) with interaction parameters $U/W = 1.4$, $J/W = -0.04$ and different temperatures T are indicated in the color bar by white triangular markers.

OP reads

$$f_{GL}[\Psi_{\mathbf{q}}] = a|\Psi_{\mathbf{q}}|^2 + \frac{b}{2}|\Psi_{\mathbf{q}}|^4 + \frac{\hbar^2}{2m^*}q^2|\Psi_{\mathbf{q}}|^2 \quad (1)$$

with $q = |\mathbf{q}|$. a , b , and m^* are the material and temperature dependent GL parameters. Here, the temperature-dependent correlation length ξ appears as the natural length scale of the amplitude mode ($\propto a$) and kinetic energy term

$$\xi(T) = \sqrt{\frac{\hbar^2}{2m^*|a|}} = \xi_0 \left(1 - \frac{T}{T_c}\right)^{-\frac{1}{2}} \quad (2)$$

with its zero temperature value ξ_0 being the coherence length [19]. The stationary point of Eq. (1) shows that the \mathbf{q} -dependent OP amplitude $|\Psi_{\mathbf{q}}| = |\Psi_{q=0}|\sqrt{1 - \xi^2 q^2}$ decreases with increasing momentum q . For large enough q , SC order breaks down (i.e., $\Psi_{\mathbf{q}} \rightarrow 0$) as the kinetic energy from phase modulations becomes comparable to

the gain in energy from pairing. The length scale associated with this breakdown is ξ and can, therefore, be inferred from the \mathbf{q} -dependent OP suppression. We employ, here, the criterion $\xi = 1/(\sqrt{2}|\mathbf{Q}|)$ with \mathbf{Q} such that $|\Psi_{\mathbf{Q}}/\Psi_0| = 1/\sqrt{2}$ [65].

The finite center-of-mass momentum of the Cooper pairs is concomitant with the flow of a charge supercurrent $\mathbf{j}_{\mathbf{q}} \propto \partial f_{\text{GL}}/\partial \mathbf{q} \propto |\Psi_{\mathbf{q}}|^2 \mathbf{q}$, see Eq. (S7) in the SM [65]. This current density is a non-monotonous function of \mathbf{q} with a maximum called depairing current density j_{dp} . It provides a theoretical upper bound to critical currents, j_c , measured in experiment. We note that careful design of SC samples is necessary for j_c reaching j_{dp} as its value crucially depends on sample geometry and defect densities [52, 96–98]. j_{dp} is related to the London penetration depth via

$$\lambda_L(T) = \sqrt{\frac{\Phi_0}{3\sqrt{3}\pi\mu_0\xi j_{\text{dp}}}} = \lambda_{L,0} \left(1 - \left(\frac{T}{T_c}\right)^4\right)^{-\frac{1}{2}} \quad (3)$$

with the magnetic flux quantum $\Phi_0 = h/2e$. The temperature dependence with the quartic power stated here is empirical [48, 52, 99, 100] and we find that it describes our calculations better than the linearized GL expectation [65].

B. Microscopic treatment

The GL analysis shows that the OP suppression and supercurrent induced by spatial phase variations from the FMP constraint connect to ξ and λ_L . In a microscopic description, we acquire the OP and supercurrent density from the components of the Nambu-Gor'kov Green function \mathcal{G} with FMP constraint. For convenience, the Nambu spinors $\psi_{\mathbf{k},\mathbf{q}}^\dagger = (c_{\mathbf{k}+\frac{\mathbf{q}}{2}\uparrow}^\dagger, c_{-\mathbf{k}+\frac{\mathbf{q}}{2}\downarrow}^\dagger)$ (with orbital indices suppressed) are introduced which now carry an additional dependence on \mathbf{q} . The corresponding Green function is a 2×2 matrix

$$\begin{aligned} \mathcal{G}_{\mathbf{q}}(\tau, \mathbf{k}) &= -\langle T_\tau \psi_{\mathbf{k},\mathbf{q}}(\tau) \psi_{\mathbf{k},\mathbf{q}}^\dagger \rangle \\ &= \begin{pmatrix} G_{\mathbf{q}}(\tau, \mathbf{k}) & F_{\mathbf{q}}(\tau, \mathbf{k}) \\ F_{\mathbf{q}}^*(\tau, \mathbf{k}) & -G_{\mathbf{q}}(-\tau, -\mathbf{k}) \end{pmatrix} \end{aligned} \quad (4)$$

in Nambu space where the normal (anomalous) Green function G (F) components on imaginary time τ take over the \mathbf{q} -dependence. Here, we use as the OP the local anomalous Green function

$$|\Psi_{\mathbf{q}}| \equiv [F_{\mathbf{q}}^{\text{loc}}(\tau = 0^-)]_{\alpha\alpha} = \sum_{\mathbf{k}} \langle c_{\alpha\mathbf{k}+\frac{\mathbf{q}}{2}\uparrow} c_{\alpha-\mathbf{k}+\frac{\mathbf{q}}{2}\downarrow} \rangle, \quad (5)$$

which is the same for all orbitals α . The current density can be calculated via (c.f. Eq. (S36) in the SM [65])

$$\mathbf{j}_{\mathbf{q}} = \frac{2e}{N_{\mathbf{k}}} \sum_{\mathbf{k}} \text{Tr}_{\alpha} \left[\underline{\mathbf{v}}(\mathbf{k}) \underline{G}_{\mathbf{q}} \left(\tau = 0^-, \mathbf{k} - \frac{\mathbf{q}}{2} \right) \right] \quad (6)$$

where $\underline{\mathbf{v}}_{\mathbf{k}} = \nabla_{\mathbf{k}} \underline{h}(\mathbf{k})$ denotes the group velocity obtained from the one-electron Hamiltonian $\underline{h}(\mathbf{k})$ and the trace runs over the orbital indices of $\underline{\mathbf{v}}_{\mathbf{k}}$ and $\underline{G}_{\mathbf{q}}$ with underlined quantities indicating matrices in orbital space; $N_{\mathbf{k}}$ is the number of momentum points and e is the elementary charge. A detailed discussion of the FMP constraint in the Nambu-Gor'kov formalism and current density are given in the SM [65].

Fig. 1 shows an example of our DMFT calculations which illustrates the generic \mathbf{q} -dependence of the OP amplitude and current density for different temperatures T . Throughout the paper, we choose \mathbf{q} parallel to a reciprocal lattice vector $\mathbf{q} = q\mathbf{b}_1$. We find a monotonous suppression of the OP with increasing q . The supercurrent initially grows linearly with q , reaches its maximum j_{dp} and then collapses upon further increase of q . Thus, both $|\Psi_{\mathbf{q}}|$ and $j_{\mathbf{q}}$ behave qualitatively as expected from the GL description. For decreasing temperature, the point where the OP gets significantly suppressed moves towards larger momenta \mathbf{q} (smaller length scales ξ), while j_{dp} increases. We indicate the points where we extract ξ and j_{dp} with gray circles connected by dashed lines.

II. SUPERCONDUCTING COHERENCE IN ALKALI-DOPED FULLERIDES

As an example system, we apply FMP superconductivity to study a degenerate three-orbital model $H = H_{\text{kin}} + H_{\text{int}}$, where H_{kin} is the kinetic energy and the electron-electron interaction is described by a local Kanamori-Hubbard interaction [101, 102]

$$H_{\text{int}} = (U - 3J) \frac{\hat{N}(\hat{N} - 1)}{2} - J \left(2\hat{S}^2 + \frac{1}{2}\hat{\mathbf{L}}^2 - \frac{5}{2}\hat{N} \right) \quad (7)$$

with total number \hat{N} , spin $\hat{\mathbf{S}}$, and angular momentum operator $\hat{\mathbf{L}}$. The independent interactions are the intra-orbital Hubbard term U and Hund exchange J , as we use the rotational $\text{SU}(2) \times \text{SO}(3)$ symmetric parametrization $U' = U - 2J$ for the interorbital interaction [102, 103].

This model is often discussed in the context of Hund's metal physics relevant to, e.g., transition-metal oxides like ruthenates with partially filled t_{2g} shells [102, 104]. In the special case of negative exchange energy $J < 0$, it has been introduced to A_3C_{60} materials [105, 106] to successfully explain superconductivity by first principles [78, 107]. In doped fullerenes, s -wave SC exists in proximity to a Mott-insulating (MI) [85, 87, 108–114] and a Jahn-Teller metallic phase [87, 115–120]. The influence of strong correlation effects [121–123] and inverted Hund's coupling were shown to be essential for the SC pairing [78, 105–107, 124–126] utilizing orbital fluctuations [127, 128] in a Suhl-Kondo mechanism [115, 129–132].

The inversion of J seems unusual from the standpoint of atomic physics, where it dictates the filling of atomic

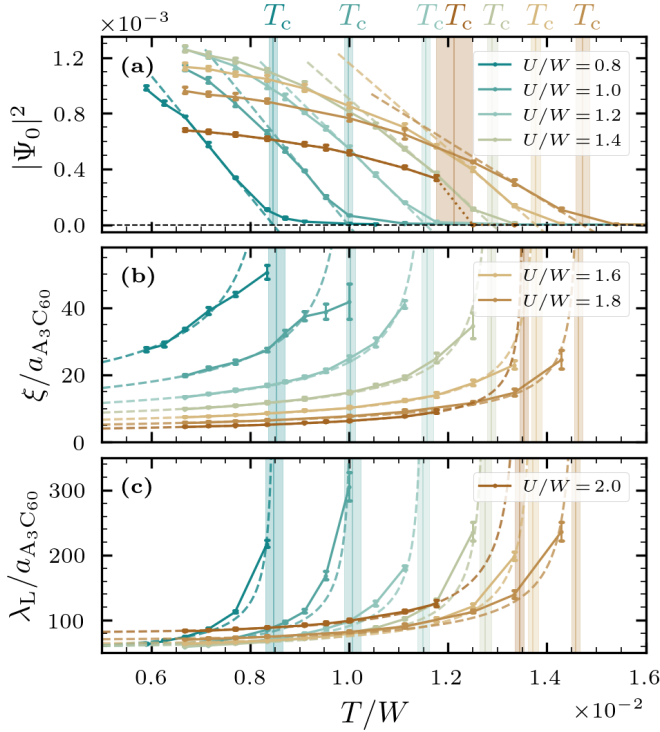


FIG. 2. Temperature dependence of (a) the zero-momentum order parameter $|\Psi_0|$, (b) correlation length ξ , and (c) London penetration depth λ_L for fixed $J/W = -0.04$ and different values of U/W . Fits to extract critical temperatures T_c and zero-temperature values ξ_0 and $\lambda_{L,0}$ are shown by dashed lines.

shells via Hund's rules. In A_3C_{60} , a negative J is induced by the electronic system coupling to intramolecular Jahn-Teller phonon modes [124, 125, 133, 134]. As a result, Hund's rules are inverted such that states which minimize first spin S and then angular momentum L are energetically most favorable [65]. This can be directly read of from the second term of Eq. (7) for $J < 0$.

A. Characteristic length scales

We connect the model to A_3C_{60} by using an *ab initio* derived Wannier construction of the half-filled t_{1u} bands for H_{kin} with the bandwidth W as the unit of energy ($W \approx 0.3 - 0.5$ eV for Cs to K based A_3C_{60}) [65, 78, 135]. For the interaction, we take first principles estimates found to describe the material well with fixed $J/W = -0.04$ and varying U/W [78, 105, 106, 118]. Different ratios U/W emulate unit cell volumes as resulting from the size of the different alkali dopands. We show the temperature dependence of $|\Psi_{q=0}|$, ξ , and λ_L for different U/W in Fig. 2.

Close to the transition point, the OP vanishes and the critical temperature T_c can be extracted from $|\Psi_0|^2 \propto T - T_c$. We find that T_c increases with U , contrary to the expectation that a repulsive interaction should be

detrimental to electron pairing. This behavior is well understood in the picture of strongly correlated superconductivity. As the correlations quench the mobility of carriers, the effective pairing interaction $\sim J/ZW$ increases due to a reduction of the quasiparticle weight Z [105, 106]. The trend of increasing T_c is broken by a first-order SC to MI phase transition for critical $U \sim 2W$ which is indicated by a dotted line. Upon approaching the MI phase, the magnitude of $|\Psi_0|$ behaves in a dome-like shape. The T_c values of $0.8 - 1.4 \times 10^{-2} W$ that we obtain from DMFT correspond to 49–85 K which is on the order of but quantitatively higher than the experimentally observed values. The reason for this is that we approximate the interaction to be instantaneous as well as that we neglect non-local correlations which reduce T_c [78].

Turning to the correlation length, we observe that, away from T_c , ξ is strongly reduced to only a few lattice constants ($a_{A_3C_{60}} \sim 14.2 - 14.5 \text{ \AA}$) by increasing U , i.e., pairing becomes very localized. At the same time, λ_L is enlarged. Hence, the condensate becomes much softer, i.e., there is a reduction of the SC stiffness $I \propto \lambda_L^{-2}$ upon increasing U . Fitting Eqs. (2) and (3) to our data, we obtain zero-temperature values of $\xi_0 = 3 - 10$ nm and $\lambda_{L,0} = 80 - 120$ nm. Comparing our results with experimental values of $\xi_0 \sim 2 - 4.5$ nm and $\lambda_L \sim 200 - 800$ nm [22–24, 136–146], we see an almost quantitative match for ξ_0 and a qualitative match for λ_L . Both experiment and theory consistently classify A_3C_{60} as type II superconductors ($\lambda \gg \xi$) [88, 123].

We speculate that disorder and spontaneous orbital-symmetry breaking [120] in the vicinity of the Mott state could lead to a further reduction of ξ_0 as well as an increase of λ_L beyond what is found here for the pure system. This could bring our calculations with minimal $\xi_0 = 3$ nm closer to the experimental minimal coherence length of 2 nm revealed by measurements of large upper critical fields reaching up to a maximal $H_{c2} = 90$ T in Ref. 146 using $H_{c2} = \Phi_0/(2\pi\xi_0)$.

B. Influence of Hund's coupling inversion

The inverted Hund's coupling is crucial for superconductivity in A_3C_{60} . This premise motivates us to explore in Fig. 3 the nature of the SC state in the interaction (U, J) phase space for $J < 0$ beyond *ab initio* estimates.

As long as $|J| < U/2$, we find that strengthening the negative Hund's coupling enhances the SC critical temperature with an increase up to $T_c \approx 5 \times 10^{-2} W$, i.e., by a factor of seven compared to the *ab initio* motivated case of $J/W = -0.04$. There is, however, a change in the role that U plays in the formation of superconductivity. While U was supportive for small magnitudes $|J| \lesssim 0.05 W$, it increasingly becomes unfavorable for $|J| > 0.05 W$ where T_c is reduced with increasing U . The effect is largest in proximity to the MI phase where SC is strongly suppressed. We indicate this region by a dashed

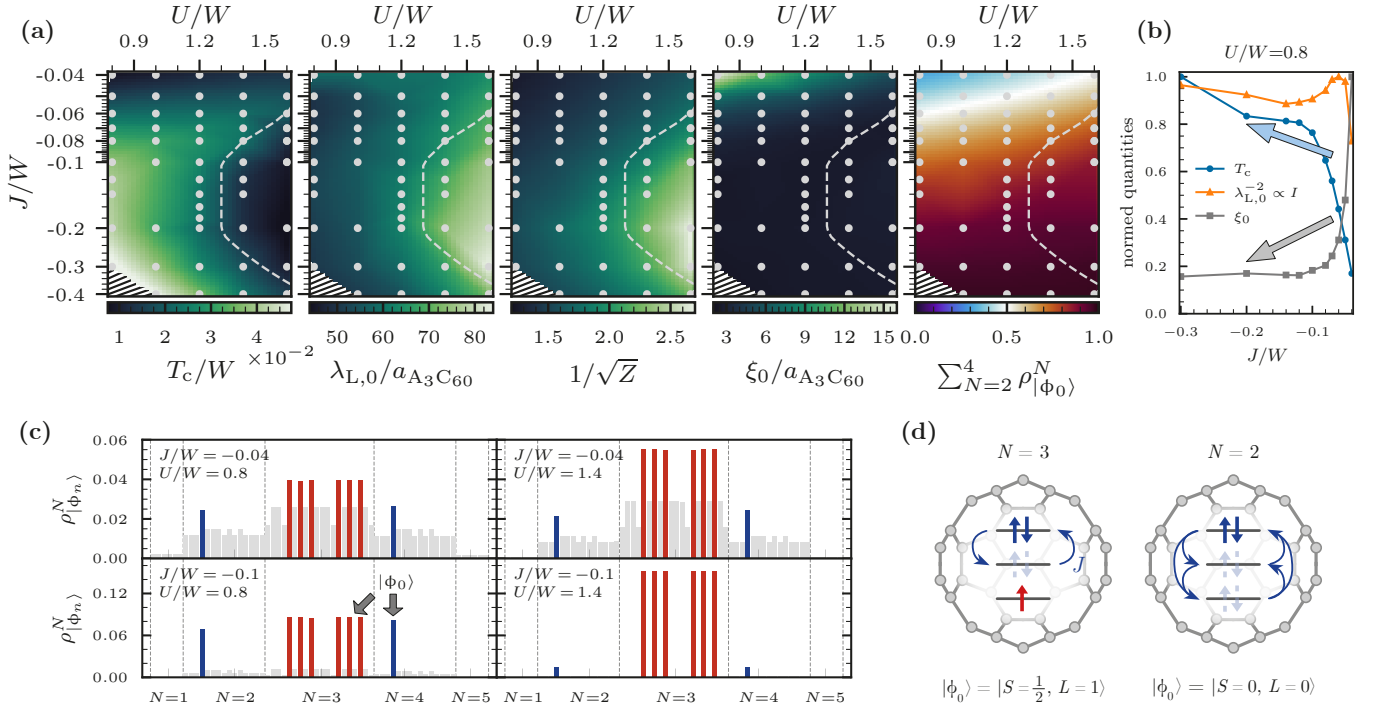


FIG. 3. Nature of the superconducting state depending on Hubbard U and inverted Hund's coupling J . (a) Critical temperature T_c , zero temperature penetration depth $\lambda_{L,0}$, inverse square root of quasiparticle weight Z , coherence length ξ_0 , and the total statistical local density matrix weight $\rho_{|\phi_0\rangle}^N$ of the local lowest energy states $|\phi_0\rangle$ of the $N = 2, 3, 4$ particle sectors obeying inverted Hund's rules [65] as a function of U and J . Dots show original data points used for interpolation and the dashed line indicates a region where the proximity to the Mott state leads to a suppression of the superconducting state. (b) Line cuts at $U/W = 0.8$ showing the opposite trends of T_c and $I \propto \lambda_{L,0}^{-2}$ compared to ξ_0 as a function of J which we indicate with arrows. Each quantity is normalized to its maximal value. (c) Distribution of statistical weights $\rho_{|\phi_n\rangle}^N$ at four different points of the phase diagrams in (a). Red (blue) bars denote the density matrix weight of ground states in the $N = 3$ ($N = 2, 4$) particle sector of which the sum is plotted in panel (a). (d) Exemplary depiction of representative lowest inverted Hund's rule eigenstates. A delocalized doublon (electron pair) exists between different orbitals due to correlated pair hopping J .

line [65].

The impact of U on the SC state can be most clearly understood from the U -dependence of the London penetration depth: λ_L grows monotonously with U and reaches its maximum close to the MI phase. Hence, the condensate is softest in the region where Mott physics is important and it becomes stiffer at smaller U . We find that this fits to the behavior of the effective bandwidth $W_{\text{eff}} = ZW \propto I$ where the quasiparticle weight Z is suppressed upon approaching the Mott phase. The behavior of Z shown in Fig. 3(a) confirms the qualitative connection $\lambda_L \propto I^{-1/2} \propto 1/\sqrt{Z}$ for $|J| > 0.05W$. The J -dependence of λ_L is much weaker than the U -dependence.

ξ_0 , in contrast, shows a very strong response to changing J . By just slightly increasing $|J|$ above the *ab initio* estimate of $|J|$, the SC state becomes strongly localized with a short coherence length on the order of $2-3 a_{\text{A}_3\text{C}_{60}}$. Remarkably, the small value of ξ_0 is independent of U and thus the proximity to the MI phase. The localization of the Cooper pairs towards ξ_0 on the order of the lattice constant is reminiscent of the BCS to BEC crossover. In the usual BCS-BEC phenomenology, T_c and the stiffness

I are suppressed in the BEC limit upon enhancing the pairing interaction and a dome-shaped T_c -dependence on the pairing strength emerges. Here, however, such a SC dome is *absent*. T_c still grows inside the plateau of minimal ξ_0 when increasing the effective pairing strength proportional to $|J|$ for fixed U/W . Only by diagonally traversing the (U, J) phase space, it is possible to suppress T_c inside the short ξ_0 plateau similar to Ref. 118. Panel Fig. 3(b) summarizes the opposite tendencies of T_c , $\lambda_{L,0}^{-2} \propto I$, and ξ_0 and the absence of a SC dome as a function of negative J for $U/W = 0.8$.

The reason for this beyond BCS-BEC physics can be understood from an analysis of the local density matrix weights $\rho_{|\phi_n\rangle}$, where $|\phi_n\rangle$ refers to the eigenstates of the local Hamiltonian of our DMFT auxiliary impurity problem. We show $\rho_{|\phi_n\rangle}$ of four different points in the interaction phase space in Fig. 3(c). In the region of short ξ_0 , the local density matrix is dominated by only eight states (red and blue bars) given by the “inverted Hund's rule” ground states $|\phi_0\rangle$ of the charge sectors with $N = 2, 3, 4$ particles that are sketched in Fig. 3(d) [65]. This can be seen in the last panel of Fig. 3(a) as the total weight

of these eight states approaches one when entering the plateau of short ξ_0 .

By increasing $|J|$, local singlets are formed as Cooper pair precursors [133] while electronic hopping is not inhibited. On the contrary, a larger negative J even facilitates hopping between the $N = 2, 3, 4$ ground states. It does so by controlling two competing energy scales: Enhancing $J < 0$ reduces the atomic gap $\Delta_{\text{at}} = E_0^{N=4} + E_0^{N=2} - 2E_0^{N=3} = U - 2|J|$ [65, 102] relevant to charge excitations and thereby supports hopping. A higher negative Hund's exchange simultaneously increases the energy $\Delta E = 2|J|$ necessary to change the spin configuration within a charge sector. As a result, unpaired electrons in the $N = 3$ state become more itinerant while Cooper pair binding becomes stronger. Since the hopping is not reduced, the SC stiffness is not compromised by larger $|J|$. The two-faced role or Janus effect of negative Hund's exchange, that localizes Cooper pairs but delocalizes electrons, can be understood as a competition of a Mott and a charge disproportionated insulator giving way for a metallic state in between [147].

Correspondingly, as the superconducting state at $-J/W > 0.05$ relies on *direct* transitions between the local inverted Hund's ground states from filling $N = 3$ to $N = 2$ and $N = 4$, the local Hubbard repulsion U has to fulfill two requirements for superconductivity with appreciable critical temperatures. First, significant occupation of the $N = 2$ and 4 states at half-filling requires that U is not too large. Otherwise, the system turns Mott insulating (around $U/W \gtrsim 1.6$) and the SC phase stiffness is reduced upon increasing U towards the Mott limit. At the same time, a significant amount of statistical weight of the $N = 3$ states demands that U must not be too small either. We find that $\Delta_{\text{at}} > 0$ and thus $U > 2|J|$ is necessary for robust SC pairing. At $\Delta_{\text{at}} < 0$ there is a predominance of $N = 2$ and 4 states, which couple kinetically only in second-order processes and which are susceptible to charge disproportionation [147]. Our analysis shows that a sweet spot for a robust SC state with high phase stiffness and large T_c exists for $|J|$ approaching $U/2$.

III. SUMMARY AND OUTLOOK

We have introduced a method to calculate the coherence length ξ_0 and the London penetration depth λ_L from the resilience of the superconducting order parameter to a FMP constraint. This approach can be implemented to any Green function or density functional based approach to superconductivity [56, 66–79] without significant increase of the numerical complexity. Thus, our work opens

the gate for “in silico” superconducting materials’ optimization targeting ξ_0 and λ_L . On a more fundamental level, availability of ξ_0 and λ_L rather than T_c alone can provide more constraints on possible pairing mechanisms through more rigorous theory-experiment comparisons, particularly in the domain of superconductors with strong electronic correlations.

For the A_3C_{60} -related multi-orbital model, our FMP-constrained DMFT studies revealed an SC regime with localized pairing and enhanced T_c upon enhancing the inverted Hund's coupling. The analysis involving ξ_0 and λ_L showed that this state stands outside the usual BCS to BEC phenomenology: A wide plateau of “minimal” coherence length is realized for $-J/W > 0.05$ inside of which T_c does not drop with further enhancement of negative J ; T_c rather still grows monotonously by up to a factor of seven. The closer analysis of the local density matrices from Fig. 3 reveals that, here, multi-orbital effects supported by the Janus effect [147] of negative J circumvent the usual BCS to BEC crossover physics.

This bypassing of the BCS-BEC scenario is promising for optimization of superconducting materials to achieve higher critical currents or temperatures, e.g., in the vicinity of the degeneracy line [147] of Mott and charge disproportionated insulators. Similarly, one can speculate under which conditions THz driving or more generally photoexcitation [39, 44–46, 89, 90] could steer A_3C_{60} into the high- T_c and short- ξ_0 plateau found here. For instance, quasiparticle trapping or some displacive meta-stability might help in realizing this superconducting state [148].

ACKNOWLEDGMENTS

We thank M. Capone, A. Cavalleri, M. Eckstein, L. Mathey, T. Nomoto, G. Rai, S. Ryee, A. Toschi, and P. Werner for fruitful discussions. NW, AIL, and TW acknowledge funding by the Cluster of Excellence ‘CUI: Advanced Imaging of Matter’ of the Deutsche Forschungsgemeinschaft (DFG) (EXC 2056, Project ID 390715994) and the DFG research unit FOR 5249 (‘QUAST’, Project No. 449872909). YN is grateful to funding via JSPS KAKENHI (No. JP23H04869 and JP21H01041). RA acknowledges funding by JSPS KAKENHI (No. JP19H05825). AIL is supported by the European Research Council via Synergy Grant 854843 - FASTCORR. The authors gratefully acknowledge the computing time granted by the Resource Allocation Board under the project hhp00056 and provided on the supercomputer Lise at NHR@ZIB as part of the NHR infrastructure. Additional calculations were performed on the Physnet cluster at the University of Hamburg.

[1] Y. Tokura, M. Kawasaki, and N. Nagaosa, Emergent functions of quantum materials, *Nature Physics* **13**,

1056 (2017).

[2] C. Yao and Y. Ma, Superconducting materials: Chal-

- allenges and opportunities for large-scale applications, *iScience* **24**, 102541 (2021).
- [3] Y. Lvovsky and P. Jarvis, Superconducting systems for MRI - present solutions and new trends, *IEEE Transactions on Applied Superconductivity* **15**, 1317 (2005).
 - [4] Y. Lvovsky, E. W. Stautner, and T. Zhang, Novel technologies and configurations of superconducting magnets for MRI, *Superconductor Science and Technology* **26**, 093001 (2013).
 - [5] J. Minervini, M. Parizh, and M. Schippers, Recent advances in superconducting magnets for MRI and hadron radiotherapy: an introduction to ‘Focus on superconducting magnets for hadron therapy and MRI’, *Superconductor Science and Technology* **31**, 030301 (2018).
 - [6] P. Schmüser, Superconductivity in high energy particle accelerators, *Progress in Particle and Nuclear Physics* **49**, 155 (2002).
 - [7] L. Rossi and L. Bottura, Superconducting Magnets for Particle Accelerators, *Reviews of Accelerator Science and Technology* **05**, 51 (2012).
 - [8] G. N. Gol’tsman, O. Okunev, G. Chulkova, A. Lipatov, A. Semenov, K. Smirnov, B. Voronov, A. Dzardanov, C. Williams, and R. Sobolewski, Picosecond superconducting single-photon optical detector, *Applied Physics Letters* **79**, 705 (2001).
 - [9] C. D. Spataru and F. Léonard, Nanoscale functionalized superconducting transport channels as photon detectors, *Physical Review B* **103**, 134512 (2021).
 - [10] F. Friedrich, P. Winkel, K. Borisov, H. Seeger, C. Sürger, I. M. Pop, and W. Wernsdorfer, Onset of phase diffusion in high kinetic inductance granular aluminum micro-SQUIDs, *Superconductor Science and Technology* **32**, 125008 (2019).
 - [11] M. I. Faley, Y. Liu, and R. E. Dunin-Borkowski, Titanium Nitride as a New Prospective Material for NanoSQUIDs and Superconducting Nanobridge Electronics, *Nanomaterials* **11**, 466 (2021).
 - [12] F. Ando, Y. Miyasaka, T. Li, J. Ishizuka, T. Arakawa, Y. Shiota, T. Moriyama, Y. Yanase, and T. Ono, Observation of superconducting diode effect, *Nature* **584**, 373 (2020).
 - [13] N. F. Q. Yuan and L. Fu, Supercurrent diode effect and finite-momentum superconductors, *Proceedings of the National Academy of Sciences* **119**, 10.1073/pnas.2119548119 (2022).
 - [14] M. Nadeem, M. S. Fuhrer, and X. Wang, The superconducting diode effect, *Nature Reviews Physics* **5**, 558 (2023).
 - [15] I. Siddiqi, Engineering high-coherence superconducting qubits, *Nature Reviews Materials* **6**, 875 (2021).
 - [16] P. W. Anderson, Plasmons, Gauge Invariance, and Mass, *Physical Review* **130**, 439 (1963).
 - [17] P. W. Higgs, Broken Symmetries and the Masses of Gauge Bosons, *Physical Review Letters* **13**, 508 (1964).
 - [18] R. Shimano and N. Tsuji, Higgs Mode in Superconductors, *Annual Review of Condensed Matter Physics* **11**, 103 (2020).
 - [19] P. Coleman, *Introduction to Many-Body Physics* (Cambridge University Press, 2008).
 - [20] Y. J. Uemura, G. M. Luke, B. J. Sternlieb, J. H. Brewer, J. F. Carolan, W. N. Hardy, R. Kadono, J. R. Kempton, R. F. Kiefl, S. R. Kreitzman, P. Mulhern, T. M. Rise-man, D. L. Williams, B. X. Yang, S. Uchida, H. Takagi, J. Gopalakrishnan, A. W. Sleight, M. A. Subramanian, C. L. Chien, M. Z. Cieplak, G. Xiao, V. Y. Lee, B. W. Statt, C. E. Stronach, W. J. Kossler, and X. H. Yu, Universal Correlations between T_c and n_s/m^* (Carrier Density over Effective Mass) in High- T_c Cuprate Superconductors, *Physical Review Letters* **62**, 2317 (1989).
 - [21] Y. J. Uemura, L. P. Le, G. M. Luke, B. J. Sternlieb, W. D. Wu, J. H. Brewer, T. M. Rise-man, C. L. Seaman, M. B. Maple, M. Ishikawa, D. G. Hinks, J. D. Jorgensen, G. Saito, and H. Yamochi, Basic similarities among cuprate, bismuthate, organic, chevre-phase, and heavy-fermion superconductors shown by penetration-depth measurements, *Physical Review Letters* **66**, 2665 (1991).
 - [22] Y. J. Uemura, A. Keren, L. P. Le, G. M. Luke, B. J. Sternlieb, W. D. Wu, J. H. Brewer, R. L. Whetten, S. M. Huang, S. Lin, R. B. Kaner, F. Diederich, S. Donovan, G. Grüner, and K. Holczer, Magnetic-field penetration depth in k3c60 measured by muon spin relaxation, *Nature* **352**, 605 (1991).
 - [23] Y. Uemura, L. Le, and G. Luke, Muon spin relaxation studies in organic superconductors and organic magnets, *Synthetic Metals* **56**, 2845 (1993).
 - [24] Y. J. Uemura, Condensation, excitation, pairing, and superfluid density in high- T_c superconductors: the magnetic resonance mode as a roton analogue and a possible spin-mediated pairing, *Journal of Physics: Condensed Matter* **16**, S4515 (2004).
 - [25] Y. J. Uemura, Dynamic superconductivity responses in photoexcited optical conductivity and Nernst effect, *Physical Review Materials* **3**, 104801 (2019).
 - [26] V. J. Emery and S. A. Kivelson, Importance of phase fluctuations in superconductors with small superfluid density, *Nature* **374**, 434 (1995).
 - [27] A. Cappellaro and L. Salasnich, Shift of the critical temperature in superconductors: a self-consistent approach, *Scientific Reports* **10**, 10.1038/s41598-020-65790-8 (2020).
 - [28] T. Timusk and B. Statt, The pseudogap in high-temperature superconductors: an experimental survey, *Reports on Progress in Physics* **62**, 61 (1999).
 - [29] M. R. Norman, D. Pines, and C. Kallin, The pseudogap: friend or foe of high T_c ?, *Advances in Physics* **54**, 715 (2005).
 - [30] P. A. Lee, N. Nagaosa, and X.-G. Wen, Doping a Mott insulator: Physics of high-temperature superconductivity, *Reviews of Modern Physics* **78**, 17 (2006).
 - [31] O. Gunnarsson, T. Schäfer, J. LeBlanc, E. Gull, J. Merino, G. Sangiovanni, G. Rohringer, and A. Toschi, Fluctuation Diagnostics of the Electron Self-Energy: Origin of the Pseudogap Physics, *Physical Review Letters* **114**, 236402 (2015).
 - [32] P. Nozières and S. Schmitt-Rink, Bose condensation in an attractive fermion gas: From weak to strong coupling superconductivity, *Journal of Low Temperature Physics* **59**, 195 (1985).
 - [33] V. M. Loktev, R. M. Quick, and S. G. Sharapov, Phase fluctuations and pseudogap phenomena, *Physics Reports* **349**, 1 (2001).
 - [34] Q. Chen, J. Stajic, S. Tan, and K. Levin, BCS-BEC crossover: From high temperature superconductors to ultracold superfluids, *Physics Reports* **412**, 1 (2005).
 - [35] J. Sous, Y. He, and S. A. Kivelson, Absence of a BCS-BEC crossover in the cuprate superconductors, *npj Quantum Materials* **8**, 10.1038/s41535-023-00550-1

- (2023).
- [36] I. Ussishkin, S. L. Sondhi, and D. A. Huse, Gaussian Superconducting Fluctuations, Thermal transport, and the Nernst Effect, *Physical Review Letters* **89**, 287001 (2002).
 - [37] M.-S. Nam, A. Ardavan, S. J. Blundell, and J. A. Schlueter, Fluctuating superconductivity in organic molecular metals close to the Mott transition, *Nature* **449**, 584 (2007).
 - [38] K. Behnia and H. Aubin, Nernst effect in metals and superconductors: a review of concepts and experiments, *Reports on Progress in Physics* **79**, 046502 (2016).
 - [39] G. Jotzu, G. Meier, A. Cantaluppi, A. Cavalleri, D. Pontiroli, M. Riccò, A. Ardavan, and M.-S. Nam, Superconducting Fluctuations Observed Far above T_c in the Isotropic Superconductor K_3C_{60} , *Physical Review X* **13**, 021008 (2023).
 - [40] A. Cavalleri, Photo-induced superconductivity, *Contemporary Physics* **59**, 31 (2017).
 - [41] D. Fausti, R. I. Tobey, N. Dean, S. Kaiser, A. Dienst, M. C. Hoffmann, S. Pyon, T. Takayama, H. Takagi, and A. Cavalleri, Light-Induced Superconductivity in a Stripe-Ordered Cuprate, *Science* **331**, 189 (2011).
 - [42] K. A. Cremin, J. Zhang, C. C. Homes, G. D. Gu, Z. Sun, M. M. Fogler, A. J. Millis, D. N. Basov, and R. D. Averitt, Photoenhanced metastable c-axis electrodynamic in stripe-ordered cuprate $La_{1.885}Ba_{0.115}CuO_4$, *Proceedings of the National Academy of Sciences* **116**, 19875 (2019).
 - [43] T. Suzuki, T. Someya, T. Hashimoto, S. Michimae, M. Watanabe, M. Fujisawa, T. Kanai, N. Ishii, J. Itatani, S. Kasahara, Y. Matsuda, T. Shibauchi, K. Okazaki, and S. Shin, Photoinduced possible superconducting state with long-lived disproportionate band filling in FeSe, *Communications Physics* **2**, 10.1038/s42005-019-0219-4 (2019).
 - [44] M. Mitrano, A. Cantaluppi, D. Nicoletti, S. Kaiser, A. Perucchi, S. Lupi, P. D. Pietro, D. Pontiroli, M. Riccò, S. R. Clark, D. Jaksch, and A. Cavalleri, Possible light-induced superconductivity in K_3C_{60} at high temperature, *Nature* **530**, 461 (2016).
 - [45] E. Rowe, B. Yuan, M. Buzzi, G. Jotzu, Y. Zhu, M. Fechner, M. Först, B. Liu, D. Pontiroli, M. Riccò, and A. Cavalleri, Resonant enhancement of photo-induced superconductivity in K_3C_{60} , *Nature Physics* 10.1038/s41567-023-02235-9 (2023).
 - [46] M. Buzzi, D. Nicoletti, M. Fechner, N. Tancogne-Dejean, M. Sentef, A. Georges, T. Biesner, E. Uykur, M. Dressel, A. Henderson, T. Siegrist, J. Schlueter, K. Miyagawa, K. Kanoda, M.-S. Nam, A. Ardavan, J. Coulthard, J. Tindall, F. Schlawin, D. Jaksch, and A. Cavalleri, Photomolecular High-Temperature Superconductivity, *Physical Review X* **10**, 031028 (2020).
 - [47] M. Buzzi, D. Nicoletti, S. Fava, G. Jotzu, K. Miyagawa, K. Kanoda, A. Henderson, T. Siegrist, J. Schlueter, M.-S. Nam, A. Ardavan, and A. Cavalleri, Phase Diagram for Light-Induced Superconductivity in κ -(ET) $_2$ -X, *Physical Review Letters* **127**, 197002 (2021).
 - [48] J. Bardeen, L. N. Cooper, and J. R. Schrieffer, Theory of Superconductivity, *Physical Review* **108**, 1175 (1957).
 - [49] S. B. Nam, Theory of Electromagnetic Properties of Superconducting and Normal Systems. I, *Physical Review* **156**, 470 (1967).
 - [50] J. W. Blezies and J. P. Carbotte, Penetration depth of V_3Si , *Physical Review B* **33**, 3509 (1986).
 - [51] M. M. Korshunov, Y. N. Togushova, and O. V. Dolgov, Impurities in multiband superconductors, *Physics-Uspekhi* **59**, 1211 (2016), *Uspekhi Fizicheskikh Nauk* **186**, 1315 (2016).
 - [52] M. Tinkham, *Introduction to superconductivity*, 2nd ed. (Dover Publications, 2004) p. 454.
 - [53] P. B. Allen, Theory of superconducting transition temperature, pair susceptibility, and coherence length, in *Modern Trends in the Theory of Condensed Matter*, edited by A. Pękalski and J. A. Przystawa (Springer Berlin Heidelberg, 2008) pp. 388–413.
 - [54] A. Toschi, M. Capone, and C. Castellani, Energetic balance of the superconducting transition across the BCS—Bose Einstein crossover in the attractive Hubbard model, *Physical Review B* **72**, 235118 (2005).
 - [55] C. Yue, S. Hoshino, A. Koga, and P. Werner, Unconventional pairing from local orbital fluctuations in strongly correlated A_3C_{60} , *Physical Review B* **104**, 075107 (2021).
 - [56] E. Gull and A. J. Millis, Superconducting and pseudogap effects on the interplane conductivity and Raman scattering cross section in the two-dimensional Hubbard model, *Physical Review B* **88**, 075127 (2013).
 - [57] O. Simard, C.-D. Hébert, A. Foley, D. Sénéchal, and A.-M. S. Tremblay, Superfluid stiffness in cuprates: Effect of Mott transition and phase competition, *Physical Review B* **100**, 094506 (2019).
 - [58] M. I. Katsnelson and A. I. Lichtenstein, First-principles calculations of magnetic interactions in correlated systems, *Physical Review B* **61**, 8906 (2000).
 - [59] M. Harland, S. Brener, A. I. Lichtenstein, and M. I. Katsnelson, Josephson lattice model for phase fluctuations of local pairs in copper oxide superconductors, *Physical Review B* **100**, 024510 (2019).
 - [60] A. I. Liechtenstein, M. I. Katsnelson, and V. A. Gubanov, Exchange interactions and spin-wave stiffness in ferromagnetic metals, *Journal of Physics F: Metal Physics* **14**, L125 (1984).
 - [61] A. Liechtenstein, M. Katsnelson, V. Antropov, and V. Gubanov, Local spin density functional approach to the theory of exchange interactions in ferromagnetic metals and alloys, *Journal of Magnetism and Magnetic Materials* **67**, 65 (1987).
 - [62] M. Fleck, A. I. Liechtenstein, A. M. Oleś, L. Hedin, and V. I. Anisimov, Dynamical Mean-Field Theory for Doped Antiferromagnets, *Physical Review Letters* **80**, 2393 (1998).
 - [63] L. M. Sandratskii, Noncollinear magnetism in itinerant-electron systems: Theory and applications, *Advances in Physics* **47**, 91 (1998).
 - [64] A. Szilva, Y. Kvashnin, E. A. Stepanov, L. Nordström, O. Eriksson, A. I. Lichtenstein, and M. I. Katsnelson, Quantitative theory of magnetic interactions in solids, *Reviews of Modern Physics* **95**, 035004 (2023).
 - [65] See the Supplemental Material (SM) available at XXX for a review of FMP superconductivity in Ginzburg-Landau theory, for a proof of the generalized Bloch theorem in Nambu space, for details of the A_3C_{60} lattice model, for a discussion of the implementation of the FMP constraint in superconducting DMFT with numerical details, for a derivation of the current density from the Nambu-Gor'kov Green function, for more details on the calculation of the coherence length ξ , de-






- pairing current j_{dp} , and London penetration depth λ_L , for an analysis of the Mott proximity region, and for a discussion of the atomic limit of the impurity problem as described by the Hubbard-Kanamori interaction with negative Hund's coupling J . The SM includes Refs. [13, 18, 19, 48, 52, 78, 92–95, 99, 100, 102, 107, 118, 135, 149–162].
- [66] B. Lilia, R. Hennig, P. Hirschfeld, G. Profeta, A. Sanna, E. Zurek, W. E. Pickett, M. Amsler, R. Dias, M. I. Eremets, C. Heil, R. J. Hemley, H. Liu, Y. Ma, C. Pierleoni, A. N. Kolmogorov, N. Rybin, D. Novoselov, V. Anisimov, A. R. Oganov, C. J. Pickard, T. Bi, R. Arita, I. Errea, C. Pellegrini, R. Requist, E. K. U. Gross, E. R. Margine, S. R. Xie, Y. Quan, A. Hire, L. Fanfarillo, G. R. Stewart, J. J. Hamlin, V. Stanev, R. S. Gonnelli, E. Piatti, D. Romanin, D. Daghero, and R. Valentí, The 2021 room-temperature superconductivity roadmap, *Journal of Physics: Condensed Matter* **34**, 183002 (2022).
- [67] L. N. Oliveira, E. K. U. Gross, and W. Kohn, Density-Functional Theory for Superconductors, *Physical Review Letters* **60**, 2430 (1988).
- [68] T. Wang, T. Nomoto, Y. Nomura, H. Shinaoka, J. Otsuki, T. Koretsune, and R. Arita, Efficient ab initio Migdal-Eliashberg calculation considering the retardation effect in phonon-mediated superconductors, *Physical Review B* **102**, 134503 (2020).
- [69] A. Davydov, A. Sanna, C. Pellegrini, J. K. Dewhurst, S. Sharma, and E. K. U. Gross, Ab initio theory of plasmonic superconductivity within the Eliashberg and density-functional formalisms, *Physical Review B* **102**, 214508 (2020).
- [70] A. Sanna, C. Pellegrini, and E. Gross, Combining Eliashberg Theory with Density Functional Theory for the Accurate Prediction of Superconducting Transition Temperatures and Gap Functions, *Physical Review Letters* **125**, 057001 (2020).
- [71] M. Imada and T. Miyake, Electronic Structure Calculation by First Principles for Strongly Correlated Electron Systems, *Journal of the Physical Society of Japan* **79**, 112001 (2010).
- [72] F. Giustino, Electron-phonon interactions from first principles, *Reviews of Modern Physics* **89**, 015003 (2017).
- [73] R. Arita, T. Koretsune, S. Sakai, R. Akashi, Y. Nomura, and W. Sano, Nonempirical Calculation of Superconducting Transition Temperatures in Light-Element Superconductors, *Advanced Materials* **29**, 1602421 (2017).
- [74] A. Georges, G. Kotliar, W. Krauth, and M. J. Rozenberg, Dynamical mean-field theory of strongly correlated fermion systems and the limit of infinite dimensions, *Reviews of Modern Physics* **68**, 13 (1996).
- [75] T. Maier, M. Jarrell, T. Pruschke, and M. H. Hettler, Quantum cluster theories, *Reviews of Modern Physics* **77**, 1027 (2005).
- [76] G. Rohringer, H. Hafermann, A. Toschi, A. Katanin, A. Antipov, M. Katsnelson, A. Lichtenstein, A. Rubtsov, and K. Held, Diagrammatic routes to nonlocal correlations beyond dynamical mean field theory, *Reviews of Modern Physics* **90**, 025003 (2018).
- [77] A. Paul and T. Birol, Applications of DFT+DMFT in Materials Science, *Annual Review of Materials Research* **49**, 31 (2019).
- [78] Y. Nomura, S. Sakai, M. Capone, and R. Arita, Unified understanding of superconductivity and Mott transition in alkali-doped fullerides from first principles, *Science Advances* **1**, 10.1126/sciadv.1500568 (2015).
- [79] M. Kitatani, L. Si, P. Worm, J. M. Tomczak, R. Arita, and K. Held, Optimizing Superconductivity: From Cuprates via Nickelates to Palladates, *Physical Review Letters* **130**, 166002 (2023).
- [80] A. F. Hebard, M. J. Rosseinsky, R. C. Haddon, D. W. Murphy, S. H. Glarum, T. T. M. Palstra, A. P. Ramirez, and A. R. Kortan, Superconductivity at 18 K in potassium-doped C_{60} , *Nature* **350**, 600 (1991).
- [81] M. J. Rosseinsky, A. P. Ramirez, S. H. Glarum, D. W. Murphy, R. C. Haddon, A. F. Hebard, T. T. M. Palstra, A. R. Kortan, S. M. Zahurak, and A. V. Makhija, Superconductivity at 28 K in Rb_xC_{60} , *Physical Review Letters* **66**, 2830 (1991).
- [82] K. Holczer, O. Klein, S. mei Huang, R. B. Kaner, K. Jian Fu, R. L. Whetten, and F. Diederich, Alkali-Fulleride Superconductors: Synthesis, Composition, and Diamagnetic Shielding, *Science* **252**, 1154 (1991).
- [83] K. Tanigaki, T. W. Ebbesen, S. Saito, J. Mizuki, J. S. Tsai, Y. Kubo, and S. Kuroshima, Superconductivity at 33 K in $Cs_xRb_yC_{60}$, *Nature* **352**, 222 (1991).
- [84] R. M. Fleming, A. P. Ramirez, M. J. Rosseinsky, D. W. Murphy, R. C. Haddon, S. M. Zahurak, and A. V. Makhija, Relation of structure and superconducting transition temperatures in A_3C_{60} , *Nature* **352**, 787 (1991).
- [85] A. Y. Ganin, Y. Takabayashi, P. Jeglič, D. Arčon, A. Potočnik, P. J. Baker, Y. Ohishi, M. T. McDonald, M. D. Tzirakis, A. McLennan, G. R. Darling, M. Takata, M. J. Rosseinsky, and K. Prassides, Polymorphism control of superconductivity and magnetism in Cs_3C_{60} close to the Mott transition, *Nature* **466**, 221 (2010).
- [86] T. Palstra, O. Zhou, Y. Iwasa, P. Sulewski, R. Fleming, and B. Zegarski, Superconductivity at 40K in cesium doped C_{60} , *Solid State Communications* **93**, 327 (1995).
- [87] R. H. Zadik, Y. Takabayashi, G. Klupp, R. H. Colman, A. Y. Ganin, A. Potočnik, P. Jeglič, D. Arčon, P. Matius, K. Kamarás, Y. Kasahara, Y. Iwasa, A. N. Fitch, Y. Ohishi, G. Garbarino, K. Kato, M. J. Rosseinsky, and K. Prassides, Optimized unconventional superconductivity in a molecular Jahn-Teller metal, *Science Advances* **1**, 10.1126/sciadv.1500059 (2015).
- [88] A. P. Ramirez, Superconductivity in alkali-doped C_{60} , *Physica C: Superconductivity and its Applications* **514**, 166 (2015).
- [89] A. Cantaluppi, M. Buzzi, G. Jotzu, D. Nicoletti, M. Mitrano, D. Pontiroli, M. Riccò, A. Perucchi, P. D. Pietro, and A. Cavalleri, Pressure tuning of light-induced superconductivity in K_3C_{60} , *Nature Physics* **14**, 837 (2018).
- [90] M. Budden, T. Gebert, M. Buzzi, G. Jotzu, E. Wang, T. Matsuyama, G. Meier, Y. Laplace, D. Pontiroli, M. Riccò, F. Schlawin, D. Jaksch, and A. Cavalleri, Evidence for metastable photo-induced superconductivity in K_3C_{60} , *Nature Physics* **17**, 611 (2021).
- [91] D. Chakraborty and A. M. Black-Schaffer, Interplay of finite-energy and finite-momentum superconducting pairing, *Physical Review B* **106**, 024511 (2022).
- [92] P. Fulde and R. A. Ferrell, Superconductivity in a Strong Spin-Exchange Field, *Physical Review* **135**, A550 (1964).
- [93] A. I. Larkin and Y. N. Ovchinnikov, Nonuniform state of superconductors, *Zh. Eksp. Teor. Fiz.* **47**, 1136 (1964).

- [94] J. J. Kinnunen, J. E. Baarsma, J.-P. Martikainen, and P. Törmä, The Fulde–Ferrell–Larkin–Ovchinnikov state for ultracold fermions in lattice and harmonic potentials: a review, *Reports on Progress in Physics* **81**, 046401 (2018).
- [95] D. F. Agterberg, J. S. Davis, S. D. Edkins, E. Fradkin, D. J. V. Harlingen, S. A. Kivelson, P. A. Lee, L. Radzihovsky, J. M. Tranquada, and Y. Wang, The Physics of Pair-Density Waves: Cuprate Superconductors and Beyond, *Annual Review of Condensed Matter Physics* **11**, 231 (2020).
- [96] C. P. Poole, R. Prozorov, H. A. Farach, and R. J. Creswick, *Superconductivity* (Elsevier, 2014).
- [97] C. C. Tsuei, J. Mannhart, and D. Dimos, Limitations on critical currents in high temperature superconductors, in *AIP Conference Proceedings* (AIP, 1989).
- [98] K. Xu, P. Cao, and J. R. Heath, Achieving the Theoretical Depairing Current Limit in Superconducting Nanomesh Films, *Nano Letters* **10**, 4206 (2010).
- [99] J. Bardeen, Theory of Superconductivity, in *Encyclopedia of Physics / Handbuch der Physik* (Springer Berlin Heidelberg, 1956) pp. 612–707.
- [100] I. Khalatnikov and A. Abrikosov, The modern theory of superconductivity, *Advances in Physics* **8**, 45 (1959).
- [101] J. Kanamori, Electron Correlation and Ferromagnetism of Transition Metals, *Progress of Theoretical Physics* **30**, 275 (1963).
- [102] A. Georges, L. de' Medici, and J. Mravlje, Strong Correlations from Hund's Coupling, *Annual Review of Condensed Matter Physics* **4**, 137 (2013).
- [103] S. Sugano, *Multiplets of transition-metal ions in crystals* (Academic Press, 1970) p. 331.
- [104] L. de' Medici, Hund's coupling and its key role in tuning multiorbital correlations, *Physical Review B* **83**, 205112 (2011).
- [105] M. Capone, M. Fabrizio, C. Castellani, and E. Tosatti, Strongly Correlated Superconductivity, *Science* **296**, 2364 (2002).
- [106] M. Capone, M. Fabrizio, C. Castellani, and E. Tosatti, Colloquium: Modeling the unconventional superconducting properties of expanded A_3C_{60} fullerenes, *Reviews of Modern Physics* **81**, 943 (2009).
- [107] Y. Nomura, S. Sakai, M. Capone, and R. Arita, Exotic s-wave superconductivity in alkali-doped fullerenes, *Journal of Physics: Condensed Matter* **28**, 153001 (2016).
- [108] Y. Takabayashi, A. Y. Ganin, P. Jeglič, D. Arčon, T. Takano, Y. Iwasa, Y. Ohishi, M. Takata, N. Takeshita, K. Prassides, and M. J. Rosseinsky, The Disorder-Free Non-BCS Superconductor Cs_3C_{60} Emerges from an Antiferromagnetic Insulator Parent State, *Science* **323**, 1585 (2009).
- [109] Y. Ihara, H. Alloul, P. Wzietek, D. Pontiroli, M. Mazzani, and M. Riccò, NMR study of the mott transitions to superconductivity in the two Cs_3C_{60} , *Physical Review Letters* **104**, 256402 (2010).
- [110] Y. Ihara, H. Alloul, P. Wzietek, D. Pontiroli, M. Mazzani, and M. Riccò, Spin dynamics at the Mott transition and in the metallic state of the Cs_3C_{60} superconducting phases, *EPL (Europhysics Letters)* **94**, 37007 (2011).
- [111] S. Kawasaki, J. Fukui, T. Motoyama, Y. Suzuki, S. Shibasaki, and G. qing Zheng, The Mott State and Superconductivity in Face-Centred Cubic structured Cs_3C_{60} : A ^{133}Cs -Nuclear Magnetic Resonance Study under Pressure, *Journal of the Physical Society of Japan* **82**, 014709 (2013).
- [112] Y. Kasahara, Y. Takeuchi, T. Itou, R. H. Zadik, Y. Takabayashi, A. Y. Ganin, D. Arčon, M. J. Rosseinsky, K. Prassides, and Y. Iwasa, Spin frustration and magnetic ordering in the $S = 1/2$ molecular antiferromagnet fcc - Cs_3C_{60} , *Physical Review B* **90**, 014413 (2014).
- [113] A. Potočník, A. Krajnc, P. Jeglič, Y. Takabayashi, A. Y. Ganin, K. Prassides, M. J. Rosseinsky, and D. Arčon, Size and symmetry of the superconducting gap in the f.c.c. Cs_3C_{60} polymorph close to the metal-Mott insulator boundary, *Scientific Reports* **4**, 10.1038/srep04265 (2014).
- [114] P. Wzietek, T. Mito, H. Alloul, D. Pontiroli, M. Aramini, and M. Riccò, NMR Study of the Superconducting Gap Variation near the Mott Transition in Cs_3C_{60} , *Physical Review Letters* **112**, 066401 (2014).
- [115] S. Suzuki, S. Okada, and K. Nakao, Theoretical Study on the Superconductivity Induced by the Dynamic Jahn-Teller Effect in Alkali-Metal-Doped C_{60} , *Journal of the Physical Society of Japan* **69**, 2615 (2000).
- [116] G. Klupp, P. Matus, K. Kamarás, A. Y. Ganin, A. McLennan, M. J. Rosseinsky, Y. Takabayashi, M. T. McDonald, and K. Prassides, Dynamic Jahn-Teller effect in the parent insulating state of the molecular superconductor Cs_3C_{60} , *Nature Communications* **3**, 10.1038/ncomms1910 (2012).
- [117] N. Iwahara and L. F. Chibotaru, Dynamical Jahn-Teller instability in metallic fullerenes, *Physical Review B* **91**, 035109 (2015).
- [118] S. Hoshino and P. Werner, Spontaneous Orbital-Selective Mott Transitions and the Jahn-Teller Metal of A_3C_{60} , *Physical Review Letters* **118**, 177002 (2017).
- [119] P. Werner, H. U. R. Strand, S. Hoshino, and M. Eckstein, Ultrafast switching of composite order in A_3C_{60} , *Physical Review B* **95**, 195405 (2017).
- [120] S. Hoshino, P. Werner, and R. Arita, Unconventional orbital ordering and emergent dimensional reduction in fullerene superconductors, *Physical Review B* **99**, 235133 (2019).
- [121] R. W. Lof, M. A. van Veenendaal, B. Koopmans, H. T. Jonkman, and G. A. Sawatzky, Band gap, excitons, and Coulomb interaction in solid C_{60} , *Physical Review Letters* **68**, 3924 (1992).
- [122] S. Chakravarty, S. Khlebnikov, and S. Kivelson, Comment on "Electron-phonon coupling and superconductivity in alkali-intercalated C_{60} solid", *Physical Review Letters* **69**, 212 (1992).
- [123] O. Gunnarsson and G. Zwicknagl, Coulomb pseudopotential, screening and superconductivity in C_{60} , *Physical Review Letters* **69**, 957 (1992).
- [124] M. Capone, M. Fabrizio, P. Giannozzi, and E. Tosatti, Theory of the metal-nonmagnetic Mott-Jahn-Teller insulator transition in A_4C_{60} , *Physical Review B* **62**, 7619 (2000).
- [125] M. Capone, M. Fabrizio, and E. Tosatti, Direct transition between a Singlet Mott Insulator and a Superconductor, *Physical Review Letters* **86**, 5361 (2001).
- [126] M. Capone, M. Fabrizio, C. Castellani, and E. Tosatti, Strongly Correlated Superconductivity and Pseudogap Phase near a Multiband Mott Insulator, *Physical Review Letters* **93**, 047001 (2004).
- [127] A. Koga and P. Werner, Superconductivity in the two-band Hubbard model, *Physical Review B* **91**, 085108

- (2015).
- [128] K. Steiner, S. Hoshino, Y. Nomura, and P. Werner, Long-range orders and spin/orbital freezing in the two-band hubbard model, *Physical Review B* **94**, 075107 (2016).
 - [129] H. Suhl, B. T. Matthias, and L. R. Walker, Bardeen-Cooper-Schrieffer Theory of Superconductivity in the Case of Overlapping Bands, *Physical Review Letters* **3**, 552 (1959).
 - [130] J. Kondo, Superconductivity in Transition Metals, *Progress of Theoretical Physics* **29**, 1 (1963).
 - [131] M. J. Rice, H. Y. Choi, and Y. R. Wang, Three-band superconductivity in K_3C_{60} and Rb_3C_{60} , *Physical Review B* **44**, 10414 (1991).
 - [132] Y. Asai and Y. Kawaguchi, Adiabatic and nonadiabatic electron-intramolecular-vibration couplings and superconductivity in fullerenes, *Physical Review B* **46**, 1265 (1992).
 - [133] J. E. Han, O. Gunnarsson, and V. H. Crespi, Strong Superconductivity with Local Jahn-Teller Phonons in C_{60} Solids, *Physical Review Letters* **90**, 167006 (2003).
 - [134] Y. Nomura and R. Arita, *Ab initio* downfolding for electron-phonon-coupled systems: Constrained density-functional perturbation theory, *Physical Review B* **92**, 245108 (2015).
 - [135] Y. Nomura, K. Nakamura, and R. Arita, Ab initio derivation of electronic low-energy models for C_{60} and aromatic compounds, *Physical Review B* **85**, 155452 (2012).
 - [136] K. Holczer, O. Klein, G. Grüner, J. D. Thompson, F. Diederich, and R. L. Whetten, Critical magnetic fields in the superconducting state of K_3C_{60} , *Physical Review Letters* **67**, 271 (1991).
 - [137] G. Sparr, J. D. Thompson, R. L. Whetten, S.-M. Huang, R. B. Kaner, F. Diederich, G. Grüner, and K. Holczer, Pressure and field dependence of superconductivity in Rb_3C_{60} , *Physical Review Letters* **68**, 1228 (1992).
 - [138] S. Foner, E. J. McNiff, D. Heiman, S.-M. Huang, and R. B. Kaner, Measurements of the upper critical field of K_3C_{60} and Rb_3C_{60} powders to 60 T, *Physical Review B* **46**, 14936 (1992).
 - [139] G. S. Boebinger, T. T. M. Palstra, A. Passner, M. J. Rosseinsky, D. W. Murphy, and I. I. Mazin, Evidence of upper-critical-field enhancement in K_3C_{60} powders, *Physical Review B* **46**, 5876 (1992).
 - [140] A. P. Ramirez, M. J. Rosseinsky, D. W. Murphy, and R. C. Haddon, Specific-heat jump at T_c and normal-state magnetic susceptibility of A_3C_{60} , *Physical Review Letters* **69**, 1687 (1992).
 - [141] L. Degiorgi, G. Grüner, P. Wachter, S.-M. Huang, J. Wiley, R. L. Whetten, R. B. Kaner, K. Holczer, and F. Diederich, Electrodynamical response of Rb_3C_{60} , *Physical Review B* **46**, 11250 (1992).
 - [142] L. Degiorgi, P. Wachter, G. Grüner, S.-M. Huang, J. Wiley, and R. B. Kaner, Optical response of the superconducting state of Rb_3C_{60} , *Physical Review Letters* **69**, 2987 (1992).
 - [143] R. Tycko, G. Dabbagh, M. J. Rosseinsky, D. W. Murphy, A. P. Ramirez, and R. M. Fleming, Electronic properties of normal and superconducting alkali fullerenes probed by ^{13}C nuclear magnetic resonance, *Physical Review Letters* **68**, 1912 (1992).
 - [144] T. T. M. Palstra, R. C. Haddon, A. F. Hebard, and J. Zaanen, Electronic transport properties of K_3C_{60} films, *Physical Review Letters* **68**, 1054 (1992).
 - [145] J. Hou, V. H. Crespi, X.-D. Xiang, W. Vareka, G. Briceño, A. Zettl, and M. L. Cohen, Determination of superconducting and normal state parameters of single crystal K_3C_{60} , *Solid State Communications* **86**, 643 (1993).
 - [146] Y. Kasahara, Y. Takeuchi, R. H. Zadik, Y. Takabayashi, R. H. Colman, R. D. McDonald, M. J. Rosseinsky, K. Prassides, and Y. Iwasa, Upper critical field reaches 90 tesla near the Mott transition in fulleride superconductors, *Nature Communications* **8**, 10.1038/ncomms14467 (2017).
 - [147] A. Isidori, M. Berović, L. Fanfarillo, L. de' Medici, M. Fabrizio, and M. Capone, Charge Disproportionation, Mixed Valence, and Janus Effect in Multiorbital Systems: A Tale of Two Insulators, *Physical Review Letters* **122**, 186401 (2019).
 - [148] S. Chattopadhyay, C. J. Eckhardt, D. M. Kennes, M. A. Sentef, D. Shin, A. Rubio, A. Cavalleri, E. A. Demler, and M. H. Michael, Mechanisms for Long-lived, Photo-Induced Superconductivity, (2023), [arXiv:2303.15355](https://arxiv.org/abs/2303.15355).
 - [149] D. Pekker and C. Varma, Amplitude/Higgs Modes in Condensed Matter Physics, *Annual Review of Condensed Matter Physics* **6**, 269 (2015).
 - [150] D.-H. Kim, J. J. Kinnunen, J.-P. Martikainen, and P. Törmä, Exotic Superfluid States of Lattice Fermions in Elongated Traps, *Physical Review Letters* **106**, 095301 (2011).
 - [151] D.-H. Kim and P. Törmä, Fulde-Ferrell-Larkin-Ovchinnikov state in the dimensional crossover between one- and three-dimensional lattices, *Physical Review B* **85**, 180508 (2012).
 - [152] M. O. J. Heikkinen, D.-H. Kim, and P. Törmä, Finite-temperature stability and dimensional crossover of exotic superfluidity in lattices, *Physical Review B* **87**, 224513 (2013).
 - [153] M. Heikkinen, D.-H. Kim, M. Troyer, and P. Törmä, Nonlocal Quantum Fluctuations and Fermionic Superfluidity in the Imbalanced Attractive Hubbard Model, *Physical Review Letters* **113**, 185301 (2014).
 - [154] K.-E. Huhtinen, M. Tylutki, P. Kumar, T. I. Vanhala, S. Peotta, and P. Törmä, Spin-imbalanced pairing and Fermi surface deformation in flat bands, *Physical Review B* **97**, 214503 (2018).
 - [155] E. Gull, A. J. Millis, A. I. Lichtenstein, A. N. Rubtsov, M. Troyer, and P. Werner, Continuous-time Monte Carlo methods for quantum impurity models, *Reviews of Modern Physics* **83**, 349 (2011).
 - [156] P. Werner, A. Comanac, L. de' Medici, M. Troyer, and A. J. Millis, Continuous-Time Solver for Quantum Impurity Models, *Physical Review Letters* **97**, 076405 (2006).
 - [157] A. A. Abrikosov, L. P. Gorkov, and I. E. Dzyaloshinski, *Methods of quantum field theory in statistical physics* (Dover Publications, 1975) p. 352.
 - [158] D. J. Scalapino, J. R. Schrieffer, and J. W. Wilkins, Strong-Coupling Superconductivity. I, *Physical Review* **148**, 263 (1966).
 - [159] T. Takimoto and T. Moriya, Theory of Spin Fluctuation-Induced Superconductivity Based on a d - p -Model. II. -Superconducting State-, *Journal of the Physical Society of Japan* **67**, 3570 (1998).
 - [160] E. Gull and A. J. Millis, Pairing glue in the two-

- dimensional hubbard model, [Physical Review B](#) **90**, 041110 (2014).
- [161] X. Dong, E. Gull, and A. J. Millis, Quantifying the role of antiferromagnetic fluctuations in the superconductivity of the doped Hubbard model, [Nature Physics](#) **18**, 1293 (2022).
- [162] A. Georges, G. Kotliar, and W. Krauth, Superconductivity in the two-band hubbard model in infinite dimensions, [Zeitschrift für Physik B Condensed Matter](#) **92**, 313 (1993).

Supplemental Material: Coherence length and penetration depth in strongly correlated superconductors

Niklas Witt ^{1,2,*} Yusuke Nomura ³ Sergey Brener,¹ Ryotaro Arita ^{4,5} Alexander I. Lichtenstein ^{1,2} and Tim O. Wehling ^{1,2,†}

¹*Institute of Theoretical Physics, University of Hamburg, Notkestraße 9-11, 22607 Hamburg, Germany*

²*The Hamburg Centre for Ultrafast Imaging, Luruper Chaussee 149, 22607 Hamburg, Germany*

³*Department of Applied Physics and Physico-Informatics,*

Keio University, 3-14-1 Hiyoshi, Kohoku-ku, Yokohama 223-8522, Japan

⁴*Research Center for Advanced Science and Technology,*

The University of Tokyo, 4-6-1 Komaba, Meguro-ku, Tokyo 153-8904, Japan

⁵*RIKEN Center for Emergent Matter Science (CEMS), 2-1 Hirosawa, Wako, Saitama 351-0198, Japan*

CONTENTS

S1. Phenomenological Ginzburg-Landau theory with finite-momentum pairing	II
A. Order parameter and supercurrent density	II
B. Relation to experimental observables	IV
S2. Generalized Bloch theorem in Nambu space	IV
S3. Lattice model for alkali-doped fullerenes	V
S4. Dynamical Mean-Field Theory under the constraint of finite-momentum pairing	VII
A. DMFT in the symmetry-broken state	VII
B. Nambu-Gor'kov formalism with finite-momentum pairing	VIII
C. Derivation of the supercurrent density	IX
D. Numerical details	XI
1. Methods and calculation parameters	XI
2. Determination of chemical potential	XI
3. Handling the Matsubara summation in the calculation of the current density	XI
4. Direction of the current	XII
S5. Details on the calculation of $ \Psi_q $, ξ , j_{dp} , and λ_L from DMFT	XIII
A. Order parameter and coherence length	XIII
B. Current density and penetration depth	XIV
C. Proximity region to Mott transition	XV
S6. Atomic limit of three-orbital model with inverted Hund's coupling	XVI
References	XVIII

* niklas.witt@physik.uni-hamburg.de

† tim.wehling@uni-hamburg.de

S1. PHENOMENOLOGICAL GINZBURG-LANDAU THEORY WITH FINITE-MOMENTUM PAIRING

The Ginzburg-Landau (GL) framework is a phenomenological (macroscopic) approach to the superconducting phase transition. Here, we illustrate with GL theory how finite-momentum pairing (FMP) of Cooper pairs connects to the intrinsic length scales of a superconductor, i.e., how introducing a FMP constraint gives access to the London penetration depth λ_L , coherence length ξ_0 , and also the depairing current j_{dp} . The GL description with FMP has been discussed in other contexts like the superconducting diode effect [S1] and Fulde-Ferrel-Larkin-Ovchinnikov (FFLO) theory [S2–S4]. Note that in this work we use the term ‘FMP’ to refer exclusively to the order parameter with a helical phase variation and constant amplitude, whereas it is sometimes also used in the context of pair density waves [S5] which imprint an amplitude modulation on the superconducting gap.

A. Order parameter and supercurrent density

We start from the GL expansion of the free energy of the symmetry-broken state in terms of the complex superconducting order parameter (OP) $\Psi(\mathbf{r}) = |\Psi(\mathbf{r})|e^{i\varphi(\mathbf{r})}$ close to the phase transition point T_c which reads

$$\mathcal{F}[\Psi] = \mathcal{F}_N + \int d^3r \left[a(T)|\Psi(\mathbf{r})|^2 + \frac{b}{2}|\Psi(\mathbf{r})|^4 + \frac{\hbar^2}{2m^*}|\nabla\Psi(\mathbf{r})|^2 \right] \quad (\text{S1})$$

where \mathcal{F}_N is the free energy of the normal state and $a(T) = \alpha(T - T_c)$ ($\alpha > 0$), $b > 0$, and m^* are the material dependent GL parameters. The GL functional encodes the two types of collective modes that emerge in the symmetry-broken state: fluctuations of the amplitude (Higgs mode) and the phase (Nambu-Goldstone mode) of the OP. The constraint of FMP means that we require the Cooper pairs to carry a finite fixed momentum \mathbf{q} , which translates to the requirement for the OP to be of the form $\Psi_{\mathbf{q}}(\mathbf{r}) = |\Psi_{\mathbf{q}}|e^{i\mathbf{q}\cdot\mathbf{r}}$. Then, the GL free energy density becomes

$$f_{\text{GL}}[\Psi_{\mathbf{q}}] = (\mathcal{F}[\Psi_{\mathbf{q}}] - \mathcal{F}_N)/V = a|\Psi_{\mathbf{q}}|^2 + \frac{b}{2}|\Psi_{\mathbf{q}}|^4 + \frac{\hbar^2 q^2}{2m^*}|\Psi_{\mathbf{q}}|^2. \quad (\text{S2})$$

The gradient term in this expression has an associated length scale which is the temperature-dependent correlation length ξ given by

$$\xi(T) = \sqrt{\frac{\hbar^2}{2m^*|a|}} = \xi_0 \left(1 - \frac{T}{T_c}\right)^{-\frac{1}{2}} \quad (\text{S3})$$

with the coherence length $\xi_0 = \hbar/\sqrt{\alpha m^* T_c}$ at $T = 0$ [S6]. The system’s stationary point is calculated from

$$\frac{\delta f_{\text{GL}}}{\delta \Psi_{\mathbf{q}}^*} = 2\Psi_{\mathbf{q}} [a(1 - \xi^2 q^2) + b|\Psi_{\mathbf{q}}|^2] \stackrel{!}{=} 0 \quad (\text{S4})$$

which results in the \mathbf{q} -dependence of the OP given by

$$|\Psi_{\mathbf{q}}|^2 = |\Psi_0|^2 (1 - \xi^2 q^2) \quad (\text{S5})$$

with the homogeneous OP $|\Psi_0|^2 = -a/b \propto T - T_c$. We plot this relation in Fig. S1(a). It shows that the OP amplitude is reduced compared to the zero momentum pairing case for any finite $q = |\mathbf{q}| > 0$. This suppression is induced by the nonlinear coupling of the Higgs mode to the phase mode [S7]. For some critical momentum value q_c , superconducting order breaks down completely ($\Psi_{q_c} = 0$) because the kinetic energy from phase modulations exceeds the gain in energy from pairing. In GL theory, this value is given exactly by $q_c = \xi^{-1}$ (c.f. Eq. (S5)), identifying the correlation length ξ as the associated length scale of this spatially induced breakdown. The temperature dependence of the OP and extracted ξ gives access to the coherence length ξ_0 via Eq. (S3) (c.f. Sec. S5 A).

The \mathbf{q} -dependence of the OP does not only give access to ξ , but at the same time connects to j_{dp} . To see this, we derive the current density in the superconducting state. For this purpose, we (briefly) introduce a vector potential \mathbf{A}

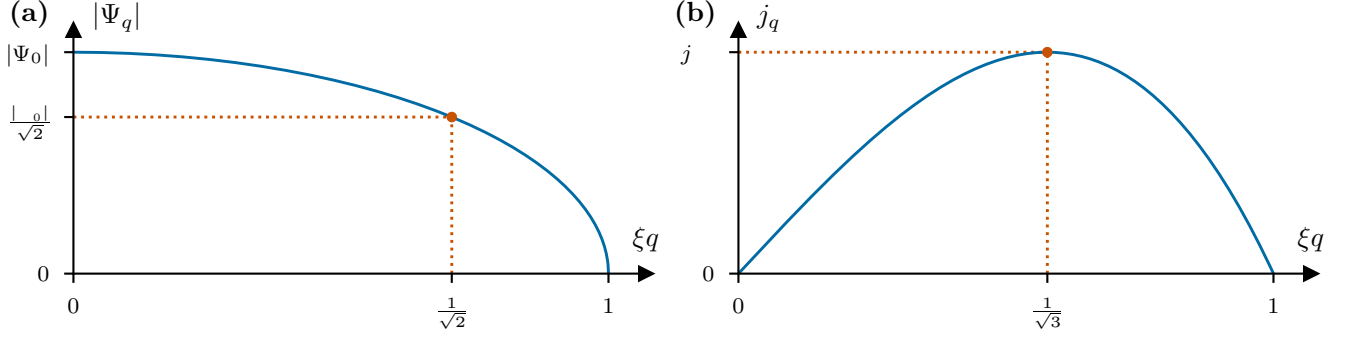


Figure S1. Ginzburg-Landau expectation of the momentum (q)-dependent (a) order parameter modulus $|\Psi_q|$ and (b) the concomitant supercurrent density j_q of a system under the constraint of finite-momentum pairing superconductivity in units of inverse correlation length ξ of. We marked the characteristic length scale on which the order parameter is reduced and the point of the depairing current density j_{dp} .

via minimal coupling to the free energy

$$\begin{aligned} f_{\text{GL}}[\Psi_{\mathbf{q}}] &= a|\Psi_{\mathbf{q}}|^2 + \frac{b}{2}|\Psi_{\mathbf{q}}|^4 + \frac{1}{2m^*}|(i\hbar\nabla + e^*\mathbf{A})\Psi_{\mathbf{q}}(\mathbf{r})|^2 \\ &= a|\Psi_{\mathbf{q}}|^2 + \frac{b}{2}|\Psi_{\mathbf{q}}|^4 + \frac{1}{2m^*}|(\hbar^2q^2 - 4\hbar e\mathbf{q} \cdot \mathbf{A} + 4e^2A^2)|\Psi_{\mathbf{q}}|^2 \end{aligned} \quad (\text{S6})$$

where we used $e^* = 2e$. We can explicitly set e^* and, in this regard, treat it differently to m^* because e^* and $(e^*)^2$ couple the same way to the OP, i.e., the charge of the Cooper pair is not renormalized. We obtain the steady-state current density from the first derivative with respect to the vector potential

$$\mathbf{j} = -\frac{\delta f_{\text{GL}}}{\delta \mathbf{A}} \Big|_{\mathbf{A}=0} = \frac{2\hbar e}{m^*}|\Psi_{\mathbf{q}}|^2 \left(\mathbf{q} - \frac{2\pi}{\Phi_0} \mathbf{A} \right) \Big|_{\mathbf{A}=0} = \frac{2\hbar e}{m^*}|\Psi_{\mathbf{q}}|^2 \mathbf{q}. \quad (\text{S7})$$

with the magnetic flux quantum $\Phi_0 = h/(2e) = \pi\hbar/e$. We set \mathbf{A} to zero although it is possible to achieve the same result by an appropriate gauge choice since the phase gradient $i\nabla\Psi_{\mathbf{q}} = -\Psi_{\mathbf{q}}\mathbf{q}$ and the vector potential are linked by gauge transformation. By inserting the OP from Eq. (S5), we obtain a \mathbf{q} -dependent expression for the current density

$$\mathbf{j}_{\mathbf{q}} = \frac{2\hbar e}{m^*}|\Psi_0|^2(1 - \xi^2q^2)\mathbf{q}\hat{\mathbf{q}}. \quad (\text{S8})$$

that directly shows how the Cooper pairs carry the supercurrent with their finite center-of-mass momentum along the direction $\hat{\mathbf{q}} = \mathbf{q}/q$. The amplitude of the current, j_q , is a non-monotonous function of q that exhibits a maximum as can be seen in Fig. S1(b). This maximum is the depairing current density, j_{dp} , beyond which the Cooper pairs start to dissolve. The value of j_{dp} can be explicitly calculated from $\partial j_q/\partial q = 0$ which yields $q_{\text{max}} = 1/(\sqrt{3}\xi)$ and

$$j_{\text{dp}} \equiv j_{q_{\text{max}}} = \frac{4}{3\sqrt{3}} \frac{\hbar e |\Psi_0|^2}{m^* \xi}. \quad (\text{S9})$$

Since the supercurrent \mathbf{j} is directly related to the vector potential \mathbf{A} , it is possible to derive the London equation within GL theory. We obtain the second London equation by taking the curl of Eq. (S7) with $\mathbf{q} = 0$ such that

$$\frac{1}{\mu_0 \lambda_L^2} \mathbf{B} = -\nabla \times \mathbf{j} = \frac{4\pi\hbar e |\Psi_0|^2}{m^* \Phi_0} \nabla \times \mathbf{A} = \frac{4e^2 |\Psi_0|^2}{m^*} \mathbf{B}. \quad (\text{S10})$$

Here, the London penetration depth λ_L is introduced which, in turn, can be reformulated to depend on the correlation

length and depairing current:

$$\lambda_L(T) = \sqrt{\frac{m^*}{4\mu_0 e^2 |\Psi_0|^2}} \stackrel{\text{Eq. (S9)}}{=} \sqrt{\frac{\Phi_0}{3\sqrt{3}\pi\mu_0 \xi j_{\text{dp}}}} = \lambda_{L,0} \left(1 - \left(\frac{T}{T_c}\right)^4\right)^{-\frac{1}{2}}. \quad (\text{S11})$$

The temperature dependence with the quartic power stated here is empirical (derived from the Gorter-Casimir model) and often used to fit experimental data [S8–S11]. In Sec. S5 B, we show that this temperature dependence models our DMFT data better than a linear power law as assumed in GL theory.

To summarize, we directly obtain the correlation length ξ and depairing current j_{dp} from introducing the FMP constraint to the OP via $\Psi_{\mathbf{q}}(\mathbf{r}) = |\Psi_{\mathbf{q}}|e^{i\mathbf{q}\cdot\mathbf{r}}$. In a second step, we can derive the London penetration depth λ_L from these two quantities. This connection also holds in microscopic theories, where we calculate the OP and current density from the Nambu-Gor'kov Green function (see Sec. S5). Lastly, we want to note that the analysis of length scales ξ and λ_L as done in this work is equivalent to discussing energy scales of Higgs and Nambu-Goldstone modes [S7, S12].

B. Relation to experimental observables

ξ , λ_L , and j_{dp} link to several experimental observables. To begin with, j_{dp} constitutes an upper theoretical bound to the critical current density, j_c , that limits the maximal current which the superconducting state of a material can endure and which is the observable measured in experiment. The value of j_c crucially depends on sample geometry and defect densities as a current only flows near the surface shell of thickness $\sim \lambda_L$.

Second, ξ and λ_L are used to scrutinize type I ($\xi \gg \lambda_L$) and type II ($\xi \ll \lambda_L$) superconductors. The reason is that they relate to critical magnetic fields: The first critical magnetic field

$$H_{c1} = \frac{\Phi_0}{4\pi\mu_0\lambda_L^2} \ln \frac{\lambda_L}{\xi} \quad (\text{S12})$$

that separates the Meissner and Abrikosov vortex lattice phases, the second critical magnetic field

$$H_{c2} = \frac{\Phi_0}{2\pi\mu_0\xi^2} \quad (\text{S13})$$

that determines the magnetic field strength boundary at which the superconductor becomes a normal metal, and the thermodynamic critical field

$$H_{c,\text{th}} = \frac{\Phi_0}{2\sqrt{2}\pi\mu_0\xi\lambda} = \sqrt{\frac{a^2}{b\mu_0}} = \sqrt{\frac{2}{\mu_0}(f_N - f_{\text{SC}})|_{\min, q=0}}. \quad (\text{S14})$$

S2. GENERALIZED BLOCH THEOREM IN NAMBU SPACE

Crystal momentum \mathbf{k} is in general not a good quantum number for systems with spatial homogeneity. This applies to the situation of an arbitrary spatially varying superconducting gap $\Delta(\mathbf{r}) = |\Delta(\mathbf{r})|e^{i\varphi(\mathbf{r})}$. In the special case of FMP with an OP of Fulde-Ferrel-type [S2], i.e., with helical phase $\varphi(\mathbf{r}) = \mathbf{q} \cdot \mathbf{r}$ and constant amplitude $|\Delta(\mathbf{r})| = |\Delta|$, however, a generalized lattice translation symmetry exists in Nambu pseudospin space that allows for the formulation of a generalized Bloch theorem. To this end, we define a generalized translation operator \mathcal{T}_n that acts on the Nambu spinor $\underline{\psi}^\dagger = (\psi_\uparrow^\dagger, \psi_\downarrow^\dagger)$ of field operators $\psi^{(\dagger)}(\mathbf{r})$:

$$\mathcal{T}_n \underline{\psi}(\mathbf{r}) = \mathcal{T}_n \begin{pmatrix} \psi_\uparrow(\mathbf{r}) \\ \psi_\downarrow(\mathbf{r}) \end{pmatrix} = \begin{pmatrix} e^{i\phi_n/2} \psi_\uparrow(\mathbf{r} + \mathbf{R}_n) \\ e^{-i\phi_n/2} \psi_\downarrow(\mathbf{r} + \mathbf{R}_n) \end{pmatrix} = e^{i\phi_n\sigma_z/2} \underline{\psi}(\mathbf{r} + \mathbf{R}_n). \quad (\text{S15})$$

Here, the spinor is not only shifted by a Bravais lattice vector \mathbf{R}_n but it is also rotated by the angle $\phi_n = \mathbf{q} \cdot \mathbf{R}_n$ along the z -axis on the Bloch sphere with σ_z being a Pauli matrix.

In the following, we show that the translation defined by Eq. (S15) leaves the Hamiltonian $H = H_0 + H_{\text{SC}}$ of a superconducting system consisting of lattice (H_0) and pairing (H_{SC}) term invariant, i.e., that it obeys a generalized Bloch theorem. In Nambu space, the Hamiltonian takes in d dimensions the form

$$\begin{aligned} H_0 + H_{\text{SC}} &= \int d^d r \left[\sum_{\sigma} \{h(\mathbf{r})\psi_{\sigma}^{\dagger}(\mathbf{r})\psi_{\sigma}(\mathbf{r})\} + \Delta_{\mathbf{q}}^*(\mathbf{r})\psi_{\uparrow}^{\dagger}(\mathbf{r})\psi_{\downarrow}^{\dagger}(\mathbf{r}) + \Delta_{\mathbf{q}}(\mathbf{r})\psi_{\downarrow}(\mathbf{r})\psi_{\uparrow}(\mathbf{r}) \right] \\ &= \int d^d r \left[\underline{\psi}^{\dagger}(\mathbf{r}) \begin{pmatrix} h(\mathbf{r}) & \Delta_{\mathbf{q}}^*(\mathbf{r}) \\ \Delta_{\mathbf{q}}(\mathbf{r}) & -h(\mathbf{r}) \end{pmatrix} \underline{\psi}(\mathbf{r}) \right] \\ &= \int d^d r \left[\underline{\psi}^{\dagger}(\mathbf{r}) (h(\mathbf{r})\sigma_z + \text{Re}\{\Delta_{\mathbf{q}}(\mathbf{r})\}\sigma_x + \text{Im}\{\Delta_{\mathbf{q}}(\mathbf{r})\}\sigma_y) \underline{\psi}(\mathbf{r}) \right] \end{aligned} \quad (\text{S16})$$

with the single-particle Hamiltonian $h(\mathbf{r}) = -\frac{\hbar^2}{2m}\nabla^2 + V(\mathbf{r})$ containing the lattice periodic potential $V(\mathbf{r}) = V(\mathbf{r} + \mathbf{R}_n)$ and with the FMP pairing potential or gap function¹ $\Delta_{\mathbf{q}}(\mathbf{r}) = |\Delta|e^{i\mathbf{q}\cdot\mathbf{r}}$. From the last line of Eq. (S16), it is immediately clear that H_0 is invariant under translation \mathcal{T}_n in Nambu space, as \mathcal{T}_n trivially commutes with $h(\mathbf{r})\sigma_z$. The invariance of H_{SC} follows from the phase shift of the pairing field $\Delta_{\mathbf{q}}(\mathbf{r} + \mathbf{R}_n) = \Delta_{\mathbf{q}}(\mathbf{r})e^{i\phi_n}$ associated with translation. This can be seen by straight-forward calculation:

$$\begin{aligned} H_{\text{SC}} &= \int d^d r \left[\underline{\psi}^{\dagger}(\mathbf{r}) \begin{pmatrix} 0 & \Delta_{\mathbf{q}}^*(\mathbf{r}) \\ \Delta_{\mathbf{q}}(\mathbf{r}) & 0 \end{pmatrix} \underline{\psi}(\mathbf{r}) \right] \\ &= \int d^d r \left[\underline{\psi}^{\dagger}(\mathbf{r} + \mathbf{R}_n) \begin{pmatrix} 0 & \Delta_{\mathbf{q}}^*(\mathbf{r} + \mathbf{R}_n) \\ \Delta_{\mathbf{q}}(\mathbf{r} + \mathbf{R}_n) & 0 \end{pmatrix} \underline{\psi}(\mathbf{r} + \mathbf{R}_n) \right] \\ &= \int d^d r \left[\underline{\psi}^{\dagger}(\mathbf{r} + \mathbf{R}_n) \begin{pmatrix} 0 & \Delta_{\mathbf{q}}^*(\mathbf{r})e^{-i\phi_n} \\ \Delta_{\mathbf{q}}(\mathbf{r})e^{i\phi_n} & 0 \end{pmatrix} \underline{\psi}(\mathbf{r} + \mathbf{R}_n) \right] \\ &= \int d^d r \left[\underline{\psi}^{\dagger}(\mathbf{r} + \mathbf{R}_n) e^{-i\phi_n\sigma_z/2} \begin{pmatrix} 0 & \Delta_{\mathbf{q}}^*(\mathbf{r}) \\ \Delta_{\mathbf{q}}(\mathbf{r}) & 0 \end{pmatrix} e^{i\phi_n\sigma_z/2} \underline{\psi}(\mathbf{r} + \mathbf{R}_n) \right] \\ &= \int d^d r \left[\underline{\psi}^{\dagger}(\mathbf{r}) \mathcal{T}_n^{\dagger} \begin{pmatrix} 0 & \Delta_{\mathbf{q}}^*(\mathbf{r}) \\ \Delta_{\mathbf{q}}(\mathbf{r}) & 0 \end{pmatrix} \mathcal{T}_n \underline{\psi}(\mathbf{r}) \right]. \end{aligned}$$

Thus, the generalized translation in Eq. (S15) is a symmetry of the system and crystal momentum \mathbf{k} constitutes a good quantum number in the case of FMP superconductivity. Note, though, that this is not true for pair density waves or generally speaking more complex FFLO-type pairings which also modulate the amplitude of the OP. In this case, methods employing supercells to accommodate for the extent of the OP modulation are necessary as was done, e.g., in Refs. [S13–S17].

S3. LATTICE MODEL FOR ALKALI-DOPED FULLERIDES

We briefly summarize the details of the Wannier-based lattice model that we use to describe the family of alkali-doped fullerenes (A_3C_{60}). The *ab initio* calculations and model derivation were done in Ref. [S18] from which we here restate the model parameters for accessibility and easier reproducibility.

The low energy subspace of A_3C_{60} materials is given by the three-orbital degenerate t_{1u} manifold. The C_{60} molecules reside on a fcc lattice and the t_{1u} bands become half-filled from doping of the alkali atoms. Generally, the lattice model takes the form

$$H_{\text{kin}} = \sum_{ij} \sum_{\alpha\gamma\sigma} t_{\alpha\gamma}(\mathbf{R}_{ij}) c_{i\alpha\sigma}^{\dagger} c_{j\gamma\sigma} = \sum_{\mathbf{k}} \sum_{\alpha\gamma\sigma} h_{\alpha\gamma}(\mathbf{k}) c_{\mathbf{k}\alpha\sigma}^{\dagger} c_{\mathbf{k}\gamma\sigma} \quad (\text{S17})$$

¹ Since $\Delta \propto \Psi$, the superconducting gap carries over the phase dependence of the order parameter under the FMP constraint.

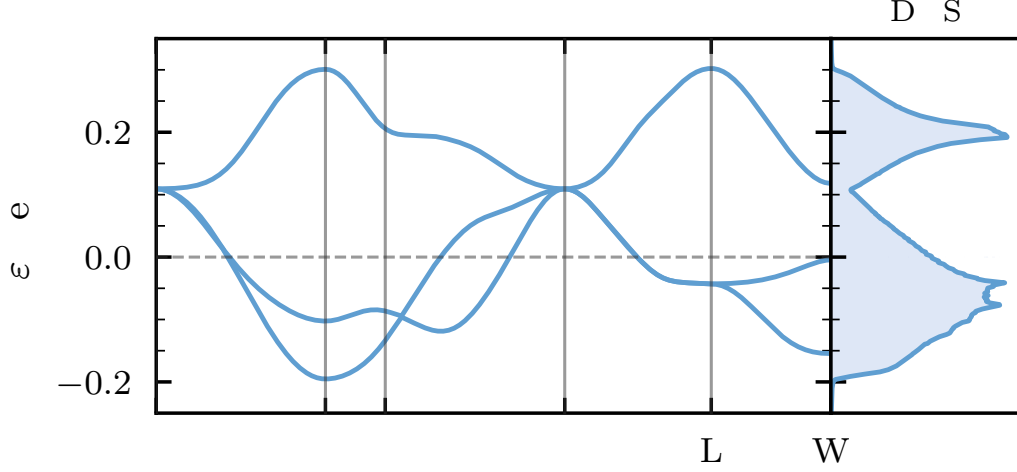


Figure S2. Band structure $\varepsilon_{\mathbf{k}}$ and density of states (DOS) of the degenerate half-filled t_{1u} bands using hopping parameters for K_3C_{60} .

with hopping terms $t_{\alpha\beta}(\mathbf{R}_{ij})$ connecting electrons on sites i, j and Wannier orbitals α, γ via $\mathbf{R}_{ij} = \mathbf{R}_i - \mathbf{R}_j$ and its Fourier transform $h_{\alpha\gamma}(\mathbf{k}) = \sum_i t_{\alpha\gamma}(\mathbf{R}_i) e^{i\mathbf{k}\mathbf{R}_i}$. $c^{(\dagger)}$ are the annihilation (creation) operators for the respective electrons with spin σ . The Wannier orbitals indicated by indices $\alpha = 1, 2, 3$ describe p_x -, p_y -, and p_z -like orbitals whose onsite energy ($\mathbf{R}_{ij} = \mathbf{0}$) is set to zero. The hopping matrices for the 12 nearest-neighbor (NN) distances are given by

$$\begin{aligned}
 & \begin{pmatrix} t_1 & t_2 & 0 \\ t_2 & t_3 & 0 \\ 0 & 0 & t_4 \end{pmatrix} \text{ for } \mathbf{R} = (0.5, 0.5, 0.0), & \begin{pmatrix} t_1 & -t_2 & 0 \\ -t_2 & t_3 & 0 \\ 0 & 0 & t_4 \end{pmatrix} \text{ for } \mathbf{R} = (0.5, -0.5, 0.0), \\
 & \begin{pmatrix} t_4 & 0 & 0 \\ 0 & t_1 & t_2 \\ 0 & t_2 & t_3 \end{pmatrix} \text{ for } \mathbf{R} = (0, 0, 0.5, 0.5), & \begin{pmatrix} t_4 & 0 & 0 \\ 0 & t_1 & -t_2 \\ 0 & -t_2 & t_3 \end{pmatrix} \text{ for } \mathbf{R} = (0, 0, 0.5, -0.5), \\
 & \begin{pmatrix} t_3 & 0 & t_2 \\ 0 & t_4 & 0 \\ t_2 & 0 & t_1 \end{pmatrix} \text{ for } \mathbf{R} = (0.5, 0, 0, 0.5), & \begin{pmatrix} t_3 & 0 & -t_2 \\ 0 & t_4 & 0 \\ -t_2 & 0 & t_1 \end{pmatrix} \text{ for } \mathbf{R} = (-0.5, 0, 0, 0.5)
 \end{aligned}$$

where the connecting lattice vectors in Cartesian coordinates $\mathbf{R}_{ij} \equiv \mathbf{R} = (R_x, R_y, R_z)$ are in units of the lattice constant $a_{\text{A}_3\text{C}_{60}}$ (see Sec. S4D4 for the definition of the lattice vectors). Hopping matrices for transfer processes to the 6 next-nearest-neighbor (NNN) sites of a C_{60} molecule are

$$\begin{pmatrix} t_5 & 0 & 0 \\ 0 & t_6 & 0 \\ 0 & 0 & t_7 \end{pmatrix} \text{ for } \mathbf{R} = (1, 0, 0), \quad \begin{pmatrix} t_7 & 0 & 0 \\ 0 & t_5 & 0 \\ 0 & 0 & t_6 \end{pmatrix} \text{ for } \mathbf{R} = (0, 1, 0), \quad \begin{pmatrix} t_6 & 0 & 0 \\ 0 & t_7 & 0 \\ 0 & 0 & t_5 \end{pmatrix} \text{ for } \mathbf{R} = (0, 0, 1)$$

The remaining NN and NNN hopping matrices can be generated from inversion symmetry $t_{\alpha\gamma}(\mathbf{R}) = t_{\alpha\gamma}(-\mathbf{R})$. In this work, we employ the Wannier construction for K_3C_{60} for which the numerical values are (in meV): $t_1 = -4$, $t_2 = -33.9$, $t_3 = 42.1$, $t_4 = -18.7$, $t_5 = -9.3$, $t_6 = -1.4$, $t_7 = -0.2$. We show the corresponding band structure (bandwidth $W \approx 0.5\text{eV}$) and density of states for the non-interacting model in Fig. S2. The main difference between different A_3C_{60} compounds is the bandwidth W and effective electronic interaction strength U [S18]. One can approximate the volume effect induced by different alkali dopands by changing the ratio U/W . The interaction Hamiltonian H_{int} is discussed in more detail in Section S6.

S4. DYNAMICAL MEAN-FIELD THEORY UNDER THE CONSTRAINT OF FINITE-MOMENTUM PAIRING

In this section, we summarize the implementation of the Dynamical Mean-Field (DMFT) calculations under the constraint of FMP. First, we summarize the ‘conventional’ approach to describe superconductivity without FMP by extending the DMFT formulation to the symmetry-broken state using the Nambu-Gor’kov formalism [S19, S20] (Sec. S4 A). Afterwards, we detail how this procedure needs to be changed to adapt the FMP constraint (Sec. S4 B) and how a charge supercurrent can be extracted (Sec. S4 C). Lastly, we summarize numerical details of our DMFT calculations (Sec. S4 D).

A. DMFT in the symmetry-broken state

We use DMFT to solve the interaction problem H_{int} (c.f. Sec. S6) of the A_3C_{60} multi-orbital lattice model H_{kin} (c.f. Sec. S3. In DMFT, the lattice model is mapped onto a single Anderson impurity problem with a self-consistent electronic bath that can be solved numerically exactly. The self-energy becomes purely local $\Sigma_{ij}(i\omega_n) = \delta_{ij}\Sigma(i\omega_n)$ capturing all local correlation effects. To this end, we have to solve the following set of self-consistent equations

$$\begin{cases} \underline{G}_{\text{loc}}(i\omega_n) = \frac{1}{N_{\mathbf{k}}} \sum_{\mathbf{k}} \underline{G}_{\mathbf{k}}(i\omega_n) = \frac{1}{N_{\mathbf{k}}} \sum_{\mathbf{k}} [(i\omega_n + \mu)\mathbb{1} - \underline{h}(\mathbf{k}) - \underline{\Sigma}(i\omega_n)]^{-1} \\ \underline{G}_{\text{W}}^{-1}(i\omega_n) = \underline{G}_{\text{loc}}^{-1}(i\omega_n) + \underline{\Sigma}(i\omega_n) \\ \underline{\Sigma}(i\omega_n) = \underline{G}_{\text{W}}^{-1}(i\omega_n) - \underline{G}_{\text{imp}}^{-1}(i\omega_n) \end{cases} \quad (\text{S18})$$

in DMFT [S20]. Here, G_{loc} is the local Green function obtained from the lattice Green function $G_{\mathbf{k}}$, G_{W} is the Weiss field, and G_{imp} is the impurity Green function; underlining denotes matrices with respect to orbital indices (α). Furthermore, $\mathbb{1}$ is the unit matrix in orbital space, $\omega_n = (2n+1)\pi T$ denote Matsubara frequencies, μ is the chemical potential, and $N_{\mathbf{k}}$ is the number of \mathbf{k} -points in the momentum mesh. Convergence of the self-consistency problem is reached when the equality $\underline{G}_{\text{loc}}(i\omega_n) = \underline{G}_{\text{imp}}(i\omega_n)$ holds.

We can study superconductivity directly in the symmetry-broken phase by extending the formalism to Nambu-Gor’kov space [S19, S20]. This can be achieved by a particle-hole transformation of the spin-down sector $c_{\mathbf{k}\alpha\downarrow}^\dagger \mapsto c_{-\mathbf{k}\alpha\downarrow}$. The result can be conveniently expressed by introducing Nambu spinors

$$\psi_{\mathbf{k},\alpha}^\dagger = \begin{pmatrix} c_{\mathbf{k}\alpha\uparrow}^\dagger & c_{-\mathbf{k}\alpha\downarrow} \end{pmatrix}, \quad \psi_{\mathbf{k},\alpha} = \begin{pmatrix} c_{\mathbf{k}\alpha\uparrow} \\ c_{-\mathbf{k}\alpha\downarrow}^\dagger \end{pmatrix} \quad (\text{S19})$$

for which the corresponding single-particle Green function (Nambu-Gor’kov Green function) becomes a 2×2 matrix in pseudospin space

$$\begin{aligned} \mathcal{G}_{\alpha\gamma}(\tau, \mathbf{k}) &= -\langle T_\tau \psi_{\mathbf{k},\alpha}(\tau) \psi_{\mathbf{k},\gamma}^\dagger \rangle = \begin{pmatrix} -\langle T_\tau c_{\mathbf{k}\alpha\uparrow}(\tau) c_{\mathbf{k}\gamma\uparrow}^\dagger \rangle & -\langle T_\tau c_{\mathbf{k}\alpha\uparrow}(\tau) c_{-\mathbf{k}\gamma\downarrow} \rangle \\ -\langle T_\tau c_{-\mathbf{k}\alpha\downarrow}^\dagger(\tau) c_{\mathbf{k}\gamma\uparrow}^\dagger \rangle & -\langle T_\tau c_{-\mathbf{k}\alpha\downarrow}^\dagger(\tau) c_{-\mathbf{k}\gamma\downarrow} \rangle \end{pmatrix} \\ &= \begin{pmatrix} G_{\alpha\gamma}(\tau, \mathbf{k}) & F_{\alpha\gamma}(\tau, \mathbf{k}) \\ F_{\alpha\gamma}^\dagger(\tau, \mathbf{k}) & \bar{G}_{\alpha\gamma}(\tau, -\mathbf{k}) \end{pmatrix} = \begin{pmatrix} G_{\alpha\gamma}(\tau, \mathbf{k}) & F_{\alpha\gamma}(\tau, \mathbf{k}) \\ F_{\alpha\gamma}^\dagger(\tau, \mathbf{k}) & -G_{\alpha\gamma}(-\tau, -\mathbf{k}) \end{pmatrix} \equiv \begin{pmatrix} \mathcal{G}_{\alpha\gamma}^{\uparrow\uparrow} & \mathcal{G}_{\alpha\gamma}^{\uparrow\downarrow} \\ \mathcal{G}_{\alpha\gamma}^{\downarrow\uparrow} & \mathcal{G}_{\alpha\gamma}^{\downarrow\downarrow} \end{pmatrix} \end{aligned} \quad (\text{S20})$$

where we used $\bar{G}(\tau, -\mathbf{k}) = -G(-\tau, -\mathbf{k})$ and F denotes the anomalous (Gor’kov) Green function. The Nambu-Gor’kov Green function takes the place of the lattice Green function $\underline{G}_{\mathbf{k}}(i\omega_n) \mapsto \underline{\mathcal{G}}(i\omega_n, \mathbf{k})$ in the self-consistency cycle (S18). It is determined from a Dyson equation where the non-interacting Green function

$$[\underline{\mathcal{G}}^0(i\omega_n, \mathbf{k})]^{-1} = \begin{pmatrix} (i\omega_n + \mu)\mathbb{1} - \underline{h}(\mathbf{k}) & 0 \\ 0 & (i\omega_n - \mu)\mathbb{1} + \underline{h}(-\mathbf{k}) \end{pmatrix} \equiv i\omega_n \mathbb{1} \cdot \sigma_0 - [\underline{h}(\mathbf{k}) - \mu\mathbb{1}] \cdot \sigma_z \quad (\text{S21})$$

and self-energy

$$\underline{\mathcal{S}}(i\omega_n) = \begin{pmatrix} \underline{\Sigma}^N(i\omega_n) & \underline{\Sigma}^{\text{AN}}(i\omega_n) \\ \underline{\Sigma}^{\text{AN}}(i\omega_n) & -[\underline{\Sigma}^N]^*(i\omega_n) \end{pmatrix} \equiv \text{Re } \underline{\Sigma}^N(i\omega_n) \cdot \sigma_z + i \text{Im } \underline{\Sigma}^N(i\omega_n) \cdot \sigma_0 + \underline{\Sigma}^{\text{AN}}(i\omega_n) \cdot \sigma_x. \quad (\text{S22})$$

also become matrices in pseudospin space which can be expressed by Pauli matrices σ_i ($i = 0, x, y, z$) for inversion symmetry $h(\mathbf{k}) = h(-\mathbf{k})$. In addition to the normal component $\Sigma^N \equiv \Sigma$, the self-energy gains an anomalous matrix element Σ^{AN} for which the gauge is chosen such that it is real-valued, i.e., only σ_x is involved in constructing \mathcal{S} . Thus, the lattice Green function in Nambu-Gor'kov space is given by

$$\begin{aligned} [\underline{\mathcal{G}}(i\omega_n, \mathbf{k})]^{-1} &= [\underline{\mathcal{G}}^0(i\omega_n, \mathbf{k})]^{-1} - \underline{\mathcal{S}}(i\omega_n) \\ &= \begin{pmatrix} (i\omega_n + \mu)\mathbb{1} - \underline{h}(\mathbf{k}) - \underline{\Sigma}^N(i\omega_n) & -\underline{\Sigma}^{\text{AN}}(i\omega_n) \\ -\underline{\Sigma}^{\text{AN}}(i\omega_n) & (i\omega_n - \mu)\mathbb{1} + \underline{h}(-\mathbf{k}) + [\underline{\Sigma}^N]^*(i\omega_n) \end{pmatrix}. \end{aligned} \quad (\text{S23})$$

The self-consistency circle (S18) generally becomes a matrix formulation in Nambu-Gor'kov space which we denote by calligraphic letters

$$\begin{cases} \underline{\mathcal{G}}_{\text{loc}}(i\omega_n) = \frac{1}{N_{\mathbf{k}}} \sum_{\mathbf{k}} \underline{\mathcal{G}}(i\omega_n, \mathbf{k}) \\ \underline{\mathcal{G}}_{\text{W}}^{-1}(i\omega_n) = \underline{\mathcal{G}}_{\text{loc}}^{-1}(i\omega_n) + \underline{\mathcal{S}}(i\omega_n) \\ \underline{\mathcal{S}}(i\omega_n) = \underline{\mathcal{G}}_{\text{W}}^{-1}(i\omega_n) - \underline{\mathcal{G}}_{\text{imp}}^{-1}(i\omega_n) \end{cases}. \quad (\text{S24})$$

B. Nambu-Gor'kov formalism with finite-momentum pairing

We now want to incorporate the FMP constraint into the Nambu-Gor'kov formalism. To treat the helical phase $e^{i\mathbf{q}\mathbf{r}}$ of the OP and gap in the framework of DMFT, several possibilities exist. For the simplest implementation, we introduce a phase gauge shift that cancels the momentum dependence of the order parameter $\Psi_{\mathbf{q}}(\mathbf{R}_i) = |\Psi|e^{i\mathbf{q}\mathbf{R}_i} = \langle c_{i\uparrow}c_{i\downarrow} \rangle$ at site \mathbf{R}_i . By applying the transformation $c_{i\alpha\sigma} \mapsto c_{i\alpha\sigma}e^{i\mathbf{q}\mathbf{R}_i/2}$ ($c_{i,\sigma}^\dagger \mapsto c_{i,\sigma}^\dagger e^{-i\mathbf{q}\mathbf{R}_i/2}$), the hopping amplitudes $t(\mathbf{R}_{ij})$ are modified to yield $\tilde{t}(\mathbf{R}_{ij}) = t(\mathbf{R}_{ij})e^{i\mathbf{q}\mathbf{R}_{ij}/2}$ such that the dispersion $\underline{\varepsilon}_{\mathbf{k}}$ obtained from diagonalizing $\underline{h}(\mathbf{k})$ is effectively replaced by $\underline{\varepsilon}_{\mathbf{k} \pm \mathbf{q}/2}$, i.e., the dispersion for up and down spins gets shifted by $\pm \mathbf{q}/2$, respectively. This shows that the introduction of FMP breaks time-reversal symmetry. The advantage of completely transferring the \mathbf{q} -dependence to the hopping matrix is that we keep the gauge freedom to choose the anomalous self-energy to be a real-valued function.

To this end, we recast Eqs. (S19) to (S23) including the FMP momentum \mathbf{q} . Through the gauge transform, the Fourier transformed creation and annihilation operators pick up the $\pm \mathbf{q}/2$ momentum shift such that the Nambu spinors obtain an additional parametric dependence

$$\psi_{\mathbf{k}, \mathbf{q}, \alpha}^\dagger = \left(c_{\mathbf{k} + \frac{\mathbf{q}}{2} \alpha \uparrow}^\dagger, c_{-\mathbf{k} + \frac{\mathbf{q}}{2} \alpha \downarrow}^\dagger \right), \quad \psi_{\mathbf{k} + \frac{\mathbf{q}}{2}, \alpha} = \begin{pmatrix} c_{\mathbf{k} + \frac{\mathbf{q}}{2} \alpha \uparrow} \\ c_{-\mathbf{k} + \frac{\mathbf{q}}{2} \alpha \downarrow} \end{pmatrix}. \quad (\text{S25})$$

The Nambu-Gor'kov Green function consequently is parametrized by \mathbf{q} as well²

$$\begin{aligned} [\underline{\mathcal{G}}_{\mathbf{q}}(\tau, \mathbf{k})]_{\alpha\gamma} &= -\langle T_\tau \psi_{\mathbf{k}, \mathbf{q}, \alpha}(\tau) \psi_{\mathbf{k}, \mathbf{q}, \gamma}^\dagger \rangle = \begin{pmatrix} -\langle T_\tau c_{\mathbf{k} + \frac{\mathbf{q}}{2} \alpha \uparrow}(\tau) c_{\mathbf{k} + \frac{\mathbf{q}}{2} \gamma \uparrow}^\dagger \rangle & -\langle T_\tau c_{\mathbf{k} + \frac{\mathbf{q}}{2} \alpha \uparrow}(\tau) c_{-\mathbf{k} + \frac{\mathbf{q}}{2} \gamma \downarrow}^\dagger \rangle \\ -\langle T_\tau c_{-\mathbf{k} + \frac{\mathbf{q}}{2} \alpha \downarrow}^\dagger(\tau) c_{\mathbf{k} + \frac{\mathbf{q}}{2} \gamma \uparrow}^\dagger \rangle & -\langle T_\tau c_{-\mathbf{k} + \frac{\mathbf{q}}{2} \alpha \downarrow}^\dagger(\tau) c_{-\mathbf{k} + \frac{\mathbf{q}}{2} \gamma \downarrow}^\dagger \rangle \end{pmatrix} \\ &= \begin{pmatrix} [\underline{\mathcal{G}}_{\mathbf{q}}(\tau, \mathbf{k})]_{\alpha\gamma} & [\underline{F}_{\mathbf{q}}(\tau, \mathbf{k})]_{\alpha\gamma} \\ [\underline{F}_{\mathbf{q}}^\dagger(\tau, \mathbf{k})]_{\alpha\gamma} & [\underline{\mathcal{G}}_{\mathbf{q}}(\tau, -\mathbf{k})]_{\alpha\gamma} \end{pmatrix} \equiv \begin{pmatrix} [\mathcal{G}_{\mathbf{q}}^{\uparrow\uparrow}]_{\alpha\gamma} & [\mathcal{G}_{\mathbf{q}}^{\uparrow\downarrow}]_{\alpha\gamma} \\ [\mathcal{G}_{\mathbf{q}}^{\downarrow\uparrow}]_{\alpha\gamma} & [\mathcal{G}_{\mathbf{q}}^{\downarrow\downarrow}]_{\alpha\gamma} \end{pmatrix}. \end{aligned} \quad (\text{S26})$$

² It is possible to define the Fourier transform of $c_i^{(\dagger)}$ differently such that the pairing is non-symmetric with respect to \mathbf{q} . Another often found notation describes Cooper pairs with electrons of momenta \mathbf{k} (in $\mathcal{G}^{\uparrow\uparrow}$) and $-\mathbf{k} + \mathbf{q}$ (in $\mathcal{G}^{\downarrow\downarrow}$) which is also the case depicted in Fig. 1 of the main text.

Note that generally $\underline{\mathcal{G}}_{\mathbf{q}}^{\uparrow\uparrow}(\tau, \mathbf{k}) \neq -\underline{\mathcal{G}}_{\mathbf{q}}^{\downarrow\downarrow}(-\tau, -\mathbf{k})$ for arbitrary, finite \mathbf{q} due to the time-reversal symmetry breaking. On Matsubara frequencies, the Nambu-Gor'kov Green function is set up via

$$[\underline{\mathcal{G}}_{\mathbf{q}}(i\omega_n, \mathbf{k})]^{-1} = \begin{pmatrix} (i\omega_n + \mu)\mathbb{1} - \underline{h}(\mathbf{k} + \frac{\mathbf{q}}{2}) - \underline{\Sigma}^{\text{N}}(i\omega_n) & -\underline{\Sigma}^{\text{AN}}(i\omega_n) \\ -\underline{\Sigma}^{\text{AN}}(i\omega_n) & (i\omega_n - \mu)\mathbb{1} + \underline{h}(-\mathbf{k} + \frac{\mathbf{q}}{2}) + [\underline{\Sigma}^{\text{N}}]^*(i\omega_n) \end{pmatrix}. \quad (\text{S27})$$

We note that the approach outlined here does not require the computationally more demanding use of supercells as, e.g., implemented in Refs. [S13–S17] to study FFLO type superconductivity.

C. Derivation of the supercurrent density

In this section, we will derive how to calculate the charge supercurrent associated with the finite center-of-mass momentum that the Cooper pairs obtain under the FMP constraint. We start with the definition of the current operator $\hat{\mathbf{j}}$. Generally, a current \mathbf{j} in a system is induced by the change of the local polarization \mathbf{P} . The polarization operator is given by

$$\hat{\mathbf{P}} = e \sum_i \mathbf{R}_i c_i^\dagger c_i = e \sum_i \mathbf{R}_i n_i \quad (\text{S28})$$

for electrons of charge e sitting at a lattice site i (we suppress orbital and spin indices for now). Then, the current is given by the time evolution (von-Neumann equation) of the polarization operator

$$\hat{\mathbf{j}} = \dot{\hat{\mathbf{P}}} = \frac{i}{\hbar} [\hat{\mathbf{P}}, H]. \quad (\text{S29})$$

We want to study the Hamiltonian with a superconducting pairing field Δ_{ij} , where we here recast Eq. (S16)

$$H = \underbrace{\sum_{ij} t_{ij} c_i^\dagger c_j}_{H_{\text{N}} \equiv H_0} + \underbrace{\sum_{ij} \Delta_{ij} c_i c_j + \Delta_{ij}^* c_j^\dagger c_i^\dagger}_{H_{\text{AN}} \equiv H_{\text{SC}}}. \quad (\text{S30})$$

for discrete lattice sites i instead of the continuous positions \mathbf{r} . To evaluate the expression (S29), we have to solve three kinds of commutators

$$\begin{aligned} [n_m, c_i^\dagger c_j] &= c_i^\dagger [n_m, c_j] + [n_m, c_i^\dagger] c_j = (\delta_{mi} - \delta_{mj}) c_i^\dagger c_j \\ [n_m, c_i c_j] &= c_i [n_m, c_j] + [n_m, c_i] c_j = -(\delta_{mi} + \delta_{mj}) c_i c_j \\ [n_m, c_i^\dagger c_j^\dagger] &= c_i^\dagger [n_m, c_j^\dagger] + [n_m, c_i^\dagger] c_j^\dagger = (\delta_{mi} + \delta_{mj}) c_i^\dagger c_j^\dagger \end{aligned}$$

where we used $[A, BC] = B[A, C] + [A, B]C$ and $[n_m, c_i^\dagger] = \delta_{im} c_i^\dagger$ ($[n_m, c_i] = -\delta_{im} c_i$). We look at the normal and anomalous component separately ($\hat{\mathbf{j}} = \hat{\mathbf{j}}_{\text{N}} + \hat{\mathbf{j}}_{\text{AN}}$):

$$\begin{aligned} \hat{\mathbf{j}}_{\text{N}} &= \frac{i}{\hbar} [\hat{\mathbf{P}}, H_{\text{N}}] = i \frac{e}{\hbar} \sum_{ijm} \mathbf{R}_m t_{ij} [n_m, c_i^\dagger c_j] = i \frac{e}{\hbar} \sum_{ijm} \mathbf{R}_m t_{ij} (\delta_{mi} - \delta_{mj}) c_i^\dagger c_j \\ &= i \frac{e}{\hbar} \sum_{ij} (\mathbf{R}_i - \mathbf{R}_j) t_{ij} c_i^\dagger c_j, \end{aligned} \quad (\text{S31})$$

$$\begin{aligned} \hat{\mathbf{j}}_{\text{AN}} &= \frac{i}{\hbar} [\hat{\mathbf{P}}, H_{\text{AN}}] = i \frac{e}{\hbar} \sum_{ijm} \mathbf{R}_m (\Delta_{ij} [n_m, c_i c_j] + \Delta_{ij}^* [n_m, c_j^\dagger c_i^\dagger]) \\ &= -i \frac{e}{\hbar} \sum_{ijm} \mathbf{R}_m (\delta_{mi} + \delta_{mj}) (\Delta_{ij} c_i c_j - \Delta_{ij}^* c_j^\dagger c_i^\dagger) \\ &= -i \frac{e}{\hbar} \sum_{ij} (\mathbf{R}_i + \mathbf{R}_j) (\Delta_{ij} c_i c_j - \Delta_{ij}^* c_j^\dagger c_i^\dagger). \end{aligned} \quad (\text{S32})$$

For calculating the current density $\mathbf{j} = \langle \hat{\mathbf{j}} \rangle$ we can make simplifications using the fact that we have local s -wave pairing in our system, i.e., $\Delta_{ij} \equiv \delta_{ij} \Delta e^{i\mathbf{q}\mathbf{R}_i}$. Since $\langle c_i c_j \rangle = -\langle c_j c_i \rangle$ and $\Delta_{ij} = \Delta_{ji}$, the expectation value of the anomalous part $\langle \hat{\mathbf{j}}_{\text{AN}} \rangle$ vanishes then.

Since the anomalous part vanishes, we only have to evaluate the normal component (S31) of the current. For this purpose, we will assume that the states at site i represent Wannier orbitals $i \rightarrow (\mathbf{R}_i, \alpha_i, \sigma_i)$ (orbital α , spin σ) which are centered on the unit cell center as is the case in the A_3C_{60} model (c.f. Sec. S3). Then, we can insert the Fourier transform of the creation and annihilation operators

$$c_i = \frac{1}{N_{\mathbf{k}}} \sum_{\mathbf{k}} \langle i | \mathbf{k} \rangle c_{\mathbf{k}} = \sum_{\mathbf{k}} e^{-i\mathbf{k}\mathbf{R}_i} \delta_{\alpha_i, \alpha_{\mathbf{k}}} \delta_{\sigma_i, \sigma_{\mathbf{k}}} c_{\mathbf{k}}, \quad c_i^\dagger = \frac{1}{N_{\mathbf{k}}} \sum_{\mathbf{k}} e^{i\mathbf{k}\mathbf{R}_i} \delta_{\alpha_i, \alpha_{\mathbf{k}}} \delta_{\sigma_i, \sigma_{\mathbf{k}}} c_{\mathbf{k}}^\dagger \quad (\text{S33})$$

to yield

$$\begin{aligned} \hat{\mathbf{j}} &= \hat{\mathbf{j}}_{\text{N}} = i \frac{e}{\hbar} \frac{1}{N_{\mathbf{k}}^2} \sum_{ij\mathbf{k}\mathbf{k}'} \delta_{\sigma_i, \sigma} \delta_{\sigma_j, \sigma'} \delta_{\alpha_i, \alpha} \delta_{\alpha_j, \alpha'} \delta_{\sigma_i, \sigma_j} [\mathbf{R}_i - \mathbf{R}_j] t_{\alpha_i \alpha_j}(\mathbf{R}_i - \mathbf{R}_j) e^{i(\mathbf{k}\mathbf{R}_i - \mathbf{k}'\mathbf{R}_j)} c_{\mathbf{k}\alpha\sigma}^\dagger c_{\mathbf{k}'\alpha'\sigma'} \\ &\stackrel{\mathbf{R}_i \mapsto \mathbf{R}_i + \mathbf{R}_j}{=} i \frac{e}{\hbar N_{\mathbf{k}}} \sum_{\substack{\mathbf{R}_i \mathbf{k} \mathbf{k}' \\ \alpha \alpha' \sigma}} \mathbf{R}_i t_{\alpha \alpha'}(\mathbf{R}_i) e^{i\mathbf{k}\mathbf{R}_i} \underbrace{\frac{1}{N_{\mathbf{k}}} \sum_{\mathbf{R}_j} e^{i(\mathbf{k} - \mathbf{k}')\mathbf{R}_j}}_{\delta_{\mathbf{k}\mathbf{k}'}} c_{\mathbf{k}\alpha\sigma}^\dagger c_{\mathbf{k}'\alpha'\sigma} \\ &= \frac{e}{\hbar N_{\mathbf{k}}} \sum_{\mathbf{k}\alpha\alpha'\sigma} i \underbrace{\sum_{\mathbf{R}_i} \mathbf{R}_i t_{\alpha \alpha'}(\mathbf{R}_i) e^{i\mathbf{k}\mathbf{R}_i}}_{=(\nabla_{\mathbf{k}} h(\mathbf{k}))_{\alpha \alpha'}} c_{\mathbf{k}\alpha\sigma}^\dagger c_{\mathbf{k}\alpha'\sigma} = \frac{e}{N_{\mathbf{k}}} \sum_{\mathbf{k}\alpha\alpha'\sigma} \mathbf{v}_{\alpha\alpha'}(\mathbf{k}) c_{\mathbf{k}\alpha\sigma}^\dagger c_{\mathbf{k}\alpha'\sigma} \end{aligned} \quad (\text{S34})$$

with the velocity $\mathbf{v}(\mathbf{k}) = \frac{1}{\hbar} \nabla_{\mathbf{k}} h(\mathbf{k})$. Thus, the current density is given by

$$\mathbf{j}_{\mathbf{q}} = \langle \hat{\mathbf{j}} \rangle_{\mathbf{q}} = \frac{e}{N_{\mathbf{k}}} \sum_{\mathbf{k}\alpha\gamma\sigma} \mathbf{v}_{\alpha\gamma}(\mathbf{k}) \langle c_{\mathbf{k}\alpha\sigma}^\dagger c_{\mathbf{k}\gamma\sigma} \rangle_{\mathbf{q}} = \frac{2e}{N_{\mathbf{k}}} \sum_{\mathbf{k}\alpha\gamma} \mathbf{v}_{\alpha\gamma}(\mathbf{k}) \langle c_{\mathbf{k}\alpha\uparrow}^\dagger c_{\mathbf{k}\gamma\uparrow} \rangle_{\mathbf{q}}. \quad (\text{S35})$$

It is straightforward to evaluate the velocity. The reduced density matrix $\langle c_{\mathbf{k}\alpha\uparrow}^\dagger c_{\mathbf{k}\gamma\uparrow} \rangle_{\mathbf{q}}$, on the other hand, can be expressed in terms of a Green function³

$$\langle c_{\mathbf{k}\alpha\uparrow}^\dagger c_{\mathbf{k}\gamma\uparrow} \rangle_{\mathbf{q}} = \left[G_{\mathbf{q}} \left(\tau = 0^-, \mathbf{k} - \frac{\mathbf{q}}{2} \right) \right]_{\gamma\alpha} = \left[\mathcal{G}_{\mathbf{q}}^{\uparrow\uparrow} \left(\tau = 0^-, \mathbf{k} - \frac{\mathbf{q}}{2} \right) \right]_{\gamma\alpha}. \quad (\text{S36})$$

The notation taken here necessitates a shift of the \mathbf{k} -mesh to fit the definition of the Nambu-Gor'kov Green function as given in Eq. (S27) for paired electrons with momenta $\mathbf{k} \pm \frac{\mathbf{q}}{2}$ (such that the dispersion entering the $\mathcal{G}^{\uparrow\uparrow}$ [$\mathcal{G}^{\downarrow\downarrow}$] component effectively carries momentum $\mathbf{k} [\mathbf{k} - \mathbf{q}]$).

Thus, we obtain an expression for the current density derived from the Nambu-Gor'kov Green function as stated in Eq.(6) of the main text⁴:

$$\mathbf{j}_{\mathbf{q}} = \frac{2e}{N_{\mathbf{k}}} \sum_{\mathbf{k}\alpha\gamma} \mathbf{v}_{\alpha\gamma}(\mathbf{k}) \left[G_{\mathbf{q}} \left(\tau = 0^-, \mathbf{k} - \frac{\mathbf{q}}{2} \right) \right]_{\gamma\alpha} = \frac{2e}{N_{\mathbf{k}}} \sum_{\mathbf{k}} \text{Tr}_{\alpha} \left[\mathbf{v}(\mathbf{k}) G \left(\tau = 0^-, \mathbf{k} - \frac{\mathbf{q}}{2} \right) \right] \quad (\text{S37})$$

In practical calculations, however, we use Eq. (S42) as this has better convergence with respect to the Matsubara summation associated with obtaining $G(\tau = 0^-)$. For details, see Sec. S4D3.

³ Instead of evaluation at $\tau = 0^-$ we can also evaluate at $\tau = 0^+$ which will result in a shift:

$G_{\beta\alpha}(\tau = 0^-) = -\langle T_{\tau} c_{\beta}(0^-) c_{\alpha}^\dagger \rangle = \langle c_{\alpha}^\dagger c_{\beta} \rangle = \delta_{\alpha\beta} - \langle c_{\beta} c_{\alpha}^\dagger \rangle = \delta_{\alpha\beta} - \langle T_{\tau} c_{\beta}(0^+) c_{\alpha}^\dagger \rangle = \delta_{\alpha\beta} + G_{\beta\alpha}(\tau = 0^+)$

⁴ We want to note that a similar expression is given above Eq. (38.13) in the book by Abrikosov, Gor'kov, and Dzyaloshinski [S21] as well as Eq. (14.245) in the book by P. Coleman [S6]. In both cases, however, it is discussed in the context of an external magnetic field \mathbf{A} .

D. Numerical details

1. Methods and calculation parameters

We use a $35 \times 35 \times 35$ \mathbf{k} -mesh and 43200 Matsubara frequencies to set up the lattice Green function in the DMFT loop. In order to solve the local impurity problem, we use a continuous-time quantum Monte Carlo (CT-QMC) solver [S22] based the strong coupling expansion in the hybridization function (CT-HYB) [S23]. Details on the implementation can be found in [S24, S25]. Depending on calculation parameters (T, U, J) and closeness to the superconducting transition, we perform between $2.4 \cdot 10^6$ up to $19.2 \cdot 10^6$ Monte Carlo sweeps and use a Legendre expansion with 50 up to 80 basis functions. Calculations very close to the onset of the superconducting phase transition (depending on temperature T or momentum \mathbf{q}) needed more than 200 DMFT iterations until convergence. We estimate an uncertainty of the Green function components by averaging over 10 or more converged DMFT iterations. This way, we can state a lower bound originating from the noise of the QMC simulation.

To induce the symmetry-breaking, we add a small pairing field $\eta = 0.1 \text{ meV}$ on the off-diagonal of the Nambu-Gor'kov Green function throughout the calculation. We keep it for the whole superconducting DMFT loop because it helps stabilizing the calculations. We checked that the presence of the small, but finite η does not change the results. In this work, we always choose $\mathbf{q} = q\mathbf{b}_1$ along the direction of a reciprocal lattice vector \mathbf{b}_1 (c.f. Sec. S4D4). The calculations with finite q are performed in practice as in the conventional case of $q = 0$ where q becomes an additional input parameter. Calculations can be sped up by first converging the DMFT loop for $q = 0$ and then using the result as a starting point for finite $q > 0$ values. We compute the \mathbf{k} -sum occurring in the expression of the supercurrent density (S37) using the same $35 \times 35 \times 35$ \mathbf{k} -mesh on 200 Matsubara frequencies.

2. Determination of chemical potential

In our calculations, we adjust the chemical potential μ in each DMFT iteration in order to keep the filling of the system fixed to $\langle n \rangle_{\mathbf{q}} = N_{\text{orb}} = 3$ for a given momentum \mathbf{q} , i.e., the t_{1u} bands are half-filled. To determine the chemical potential, we solve the following equation

$$\begin{aligned}
 \langle n \rangle_{\mathbf{q}} &= \frac{1}{N_{\mathbf{k}}} \sum_{\mathbf{k}\alpha\sigma} \langle c_{\mathbf{k}+\frac{\mathbf{q}}{2}\alpha\sigma}^\dagger c_{\mathbf{k}+\frac{\mathbf{q}}{2}\alpha\sigma} \rangle = \frac{1}{N_{\mathbf{k}}} \sum_{\mathbf{k}\alpha} \langle c_{\mathbf{k}+\frac{\mathbf{q}}{2}\alpha\uparrow}^\dagger c_{\mathbf{k}+\frac{\mathbf{q}}{2}\alpha\uparrow} \rangle + \langle c_{-\mathbf{k}+\frac{\mathbf{q}}{2}\alpha\downarrow}^\dagger c_{-\mathbf{k}+\frac{\mathbf{q}}{2}\alpha\downarrow} \rangle \\
 &= \frac{1}{N_{\mathbf{k}}} \sum_{\mathbf{k}\alpha} \langle 1 - c_{\mathbf{k}+\frac{\mathbf{q}}{2}\alpha\uparrow} c_{\mathbf{k}+\frac{\mathbf{q}}{2}\alpha\uparrow}^\dagger \rangle + \langle c_{-\mathbf{k}+\frac{\mathbf{q}}{2}\alpha\downarrow}^\dagger c_{-\mathbf{k}+\frac{\mathbf{q}}{2}\alpha\downarrow} \rangle \\
 &= N_{\text{orb}} + \frac{1}{N_{\mathbf{k}}} \sum_{\mathbf{k}\alpha} [G_{\mathbf{q}}(\tau = 0^+, \mathbf{k}) - \bar{G}_{\mathbf{q}}(\tau = 0^+, \mathbf{k})]_{\alpha\alpha} \\
 &= N_{\text{orb}} + \frac{1}{N_{\mathbf{k}}} \sum_{\mathbf{k}\omega_n} \text{Tr}_{\alpha} [\mathcal{G}_{\mathbf{q}}^{\uparrow\uparrow} - \mathcal{G}_{\mathbf{q}}^{\downarrow\downarrow}] (i\omega_n, \mathbf{k}) e^{i\omega_n 0^+}
 \end{aligned} \tag{S38}$$

In the second step, we relabeled momenta $\mathbf{k} \mapsto \mathbf{k} + \mathbf{q}$ for the spin down sector. Taking the difference $\mathcal{G}_{\mathbf{q}}^{\uparrow\uparrow} - \mathcal{G}_{\mathbf{q}}^{\downarrow\downarrow}$ helps with the convergence of the Matsubara sum to evaluate the Green functions at $\tau = 0^+$ since the frequency tail becomes $\mathcal{O}(1/(i\omega_n)^2)$.

3. Handling the Matsubara summation in the calculation of the current density

The expression for the current density, Eq. (S37), contains a Matsubara sum of the up-spin Nambu-Gor'kov Green function component $\mathcal{G}^{\uparrow\uparrow} = G$ to compute the reduced density matrix $\langle c_{\mathbf{k}\alpha\uparrow}^\dagger c_{\mathbf{k}\gamma\uparrow} \rangle_{\mathbf{q}}$ (c.f. Eq. (S36)). The Green function typically has slow convergence of Matsubara frequencies due to $1/(i\omega_n)$ -tail at high frequencies. We can achieve better convergence by including the inverse of the diagonal part of the Nambu Gor'kov Green function, i.e., the inverse of non-interacting Green function with the normal self-energy. Generally, we can expand the full Nambu Gor'kov Green

function from Eq. (S27) in terms of Pauli matrices

$$\underline{\mathcal{G}}^{-1} = \underline{g}_0 \sigma_0 + \underline{g}_z \sigma_z + \underline{g}_x \sigma_x . \quad (\text{S39})$$

We now define

$$\underline{\mathcal{G}}_{\text{N}}^{-1} = \underline{g}_0 \sigma_0 + \underline{g}_z \sigma_z \quad \text{and} \quad \underline{\mathcal{G}}_{\Delta}^{-1} = \underline{g}_x \sigma_x . \quad (\text{S40})$$

Due to charge neutrality, the following term

$$\sum_{\mathbf{k}} \text{Tr}_{\alpha} \left[\underline{\mathbf{v}}(\mathbf{k}) \underline{\mathcal{G}}_{\text{N}}^{\uparrow\uparrow} \left(\tau = 0^-, \mathbf{k} - \frac{\mathbf{q}}{2} \right) \right] = 0 \quad (\text{S41})$$

has to vanish. It evidences that the charge supercurrent is induced by the superconducting condensate which only contributes to the full Nambu Green function \mathcal{G} via the anomalous self-energy contained in $\mathcal{G}_{\Delta}^{-1}$ since $\underline{g}_x \equiv \underline{\Sigma}_{\text{AN}}$. Then, we can subtract this term from the current to obtain

$$\mathbf{j} = \frac{2e}{N_{\mathbf{k}}} \sum_{\mathbf{k}} \text{Tr}_{\alpha} \left[\underline{\mathbf{v}}(\mathbf{k}) \{ \underline{\mathcal{G}} - \underline{\mathcal{G}}_{\text{N}} \}^{\uparrow\uparrow} \left(\tau = 0^-, \mathbf{k} - \frac{\mathbf{q}}{2} \right) \right] = \frac{2e}{N_{\mathbf{k}}} \sum_{\mathbf{k}} \text{Tr}_{\alpha} \left[\underline{\mathbf{v}}(\mathbf{k}) \delta \underline{\mathcal{G}}^{\uparrow\uparrow} \left(\tau = 0^-, \mathbf{k} - \frac{\mathbf{q}}{2} \right) \right] \quad (\text{S42})$$

which has a better convergence with respect to Matsubara frequencies, since $\delta \mathcal{G}^{\uparrow\uparrow} \propto 1/(\omega_n)^3$ at large frequencies. To see the convergence behavior, we do a Taylor expansion where we focus on the pseudospin dependence only:

$$\begin{aligned} \delta \mathcal{G} &= \mathcal{G} - \mathcal{G}_{\text{N}} = (\mathcal{G}_{\text{N}}^{-1} + \mathcal{G}_{\Delta}^{-1})^{-1} - \mathcal{G}_{\text{N}} = \mathcal{G}_{\text{N}} (\sigma_0 + \mathcal{G}_{\Delta}^{-1} \mathcal{G}_{\text{N}})^{-1} - \mathcal{G}_{\text{N}} \\ &= \mathcal{G}_{\text{N}} (\sigma_0 + \mathcal{G}_{\Delta}^{-1} \mathcal{G}_{\text{N}} + \mathcal{G}_{\Delta}^{-1} \mathcal{G}_{\text{N}} \mathcal{G}_{\Delta}^{-1} \mathcal{G}_{\text{N}} + \dots) - \mathcal{G}_{\text{N}} \\ &= \mathcal{G}_{\text{N}} \mathcal{G}_{\Delta}^{-1} \mathcal{G}_{\text{N}} + \mathcal{G}_{\text{N}} \mathcal{G}_{\Delta}^{-1} \mathcal{G}_{\text{N}} \mathcal{G}_{\Delta}^{-1} \mathcal{G}_{\text{N}} + \dots \end{aligned}$$

The first term does not have any diagonal components since $\mathcal{G}_{\text{N}} = 1/\mathcal{G}_{\text{N}}^{-1} \propto \dots \sigma_0 + \dots \sigma_z$ and $\mathcal{G}_{\Delta}^{-1} \propto \sigma_x$ such that their product

$$\mathcal{G}_{\text{N}} \mathcal{G}_{\Delta}^{-1} \mathcal{G}_{\text{N}} \propto \dots \sigma_x + \dots \sigma_x \sigma_z \propto \dots \sigma_x + \dots \sigma_y . \quad (\text{S43})$$

has only off-diagonal components. Hence, the lowest order term contributing to the $\uparrow\uparrow$ component of $\delta \mathcal{G}$ is $\mathcal{O}(\mathcal{G}_{\text{N}}^3 \mathcal{G}_{\Delta}^2)$ which has an $1/(\omega_n)^3$ -tail from \mathcal{G}_{N}^3 . The Taylor expansion shows that \mathcal{G}_{N} is the zero-order term that causes the overall $1/(\omega_n)$ -tail of \mathcal{G} which we mitigate with Eq. (S42).⁵

4. Direction of the current

Here, we comment on calculating the velocity and the direction of the current. In our calculations, we employ the analytical expression for the velocity

$$\hbar \underline{\mathbf{v}}(\mathbf{k}) = \nabla_{\mathbf{k}} \hbar(\mathbf{k}) = \nabla_{\mathbf{k}} \sum_{\mathbf{R}} \underline{t}(\mathbf{R}) e^{i\mathbf{k}\mathbf{R}} = i \sum_{\mathbf{R}} \mathbf{R} \underline{t}(\mathbf{R}) e^{i\mathbf{k}\mathbf{R}} . \quad (\text{S44})$$

instead of numerically evaluating the gradient of $\hbar(\mathbf{k})$. The direction of the velocity and, hence, the supercurrent can be used as an internal consistency check of the code. In the case of A_3C_{60} , we study a fcc lattice where we construct

⁵ An approximate expression for the current utilizing the Taylor expansion up to lowest order can be found in Eq. (38.13) in the book by Abrikosov, Gor'kov, and Dzyaloshinski [S21].

Bravais lattice vectors and momenta as

$$\mathbf{R} = \sum_{i=1}^3 n_i \mathbf{a}_i, \quad \mathbf{k} = \sum_{i=1}^3 k_i \mathbf{b}_i \quad (\text{S45})$$

where we choose the lattice and corresponding reciprocal lattice vectors to be

$$\mathbf{a}_1 = \frac{a}{2}(\hat{x} + \hat{y}), \quad \mathbf{a}_2 = \frac{a}{2}(\hat{y} + \hat{z}), \quad \mathbf{a}_3 = \frac{a}{2}(\hat{x} + \hat{z}), \quad (\text{S46})$$

$$\mathbf{b}_1 = \frac{2\pi}{a}(\hat{x} + \hat{y} - \hat{z}), \quad \mathbf{b}_2 = \frac{2\pi}{a}(-\hat{x} + \hat{y} + \hat{z}), \quad \mathbf{b}_3 = \frac{2\pi}{a}(\hat{x} - \hat{y} + \hat{z}). \quad (\text{S47})$$

\hat{x}, \hat{y} , and \hat{z} are the Cartesian unit vectors. In all calculations, we put the FMP momentum \mathbf{q} parallel to one of the reciprocal lattice vectors: $\mathbf{q} = q\mathbf{b}_1 = \frac{2\pi q}{a}(\hat{x} + \hat{y} - \hat{z})$ such that in Cartesian coordinates $q_x = q_y = -q_z$. On the other hand, we determine \mathbf{j} in terms of lattice vectors \mathbf{a}_n . The condition of $\mathbf{j} \parallel \mathbf{q}$ demands that

$$\mathbf{j} = j_1 \mathbf{a}_1 + j_2 \mathbf{a}_2 + j_3 \mathbf{a}_3 \stackrel{!}{=} j(\mathbf{x} + \mathbf{y} - \mathbf{z}) \quad (\text{S48})$$

$$= a(j_1 + j_3)\hat{x} + a(j_1 + j_2)\hat{y} + a(j_2 + j_3)\hat{z} \quad (\text{S49})$$

$$\Leftrightarrow j_3 = j_2 = -\frac{1}{3}j_1 \quad (\text{S50})$$

To have the correct sign of the direction, we need $j_1 > 0$ (i.e., $j_2, j_3 < 0$). Since the fcc lattice has a very high symmetry, we can approximately treat the system to be isotropic. Because of this, we discuss in Fig. 1 of the main text and in Sec S5 B only the absolute value of the current given by $|\mathbf{j}| = 2\sqrt{3}ax$ with $x = |j_2| = |j_3| = j_1/3$.

S5. DETAILS ON THE CALCULATION OF $|\Psi_q|$, ξ , j_{dp} , AND λ_L FROM DMFT

In this section, we illustrate how the order parameter $|\Psi_q|$ and concomitantly the coherence length ξ (c.f. S5 A) as well as the depairing current j_{dp} and London penetration depth λ_L (c.f. S5 B) are obtained from the \mathbf{q} -dependence of the Nambu-Gor'kov Green function in practice. Furthermore, we elaborate on how the critical temperature extracted from the temperature dependence of ξ and λ_L can be used to scrutinize the proximity region of the Mott insulating phase and how it impacts the superconducting region (c.f. Sec. S5 C and Fig. 3 of the main text).

A. Order parameter and coherence length

Generally, the superconducting order parameter carries an orbital dependence. The superconducting pairing in A_3C_{60} , however, is orbital diagonal. Because of this, we perform an orbital average over the self-energy components Σ^{N} and Σ^{AN} in each iteration step of the DMFT loop such that they are diagonal matrices in orbital space with degenerate entries ($\Sigma_{\alpha\gamma}^{(\text{A})\text{N}} = \delta_{\alpha\gamma} \Sigma^{(\text{A})\text{N}}$). As a result, we explicitly prevent spontaneous orbital symmetry breaking in the normal self-energy [S26] and the anomalous Green function F also becomes a degenerate, diagonal matrix in orbital space. This allows us to work with a single-component OP for which we take the local anomalous Green function⁶ (c.f. Eq. (5) of the main text)

$$|\Psi_{\mathbf{q}}| \equiv [F_{\mathbf{q}}^{\text{loc}}(\tau = 0^-)]_{\alpha\alpha} = \sum_{\mathbf{k}} \langle c_{\alpha\mathbf{k}+\frac{\mathbf{q}}{2}\uparrow} c_{\alpha-\mathbf{k}+\frac{\mathbf{q}}{2}\downarrow} \rangle. \quad (\text{S51})$$

⁶ Another option to define the OP is the superconducting gap $\Delta = Z\Sigma^{\text{AN}}$ that can be calculated from the anomalous self-energy Σ^{AN} and quasiparticle weight Z [S27–S30]. Since, here, F and Δ are orbital diagonal, they can be equivalently used for defining the OP as they have the same \mathbf{q} - and T -dependence. Taking Δ as the OP would change the relative scaling of the GL free energy because of $\Delta \approx \mathcal{U}_{\text{eff}} F$ with an effective pairing potential \mathcal{U}_{eff} which is not of importance for determining ξ from the OP.

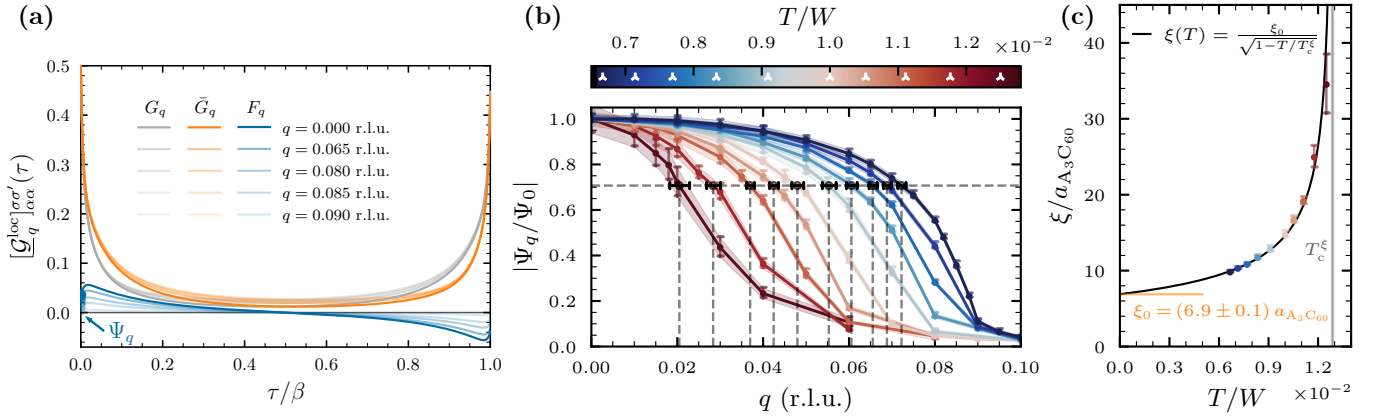


Figure S3. Extraction of the order parameter $|\Psi_q|$ and coherence length ξ from the local anomalous Green function F^{loc} . Shown data are results of the DMFT calculations for $U/W = 1.4$ and $J/W = -0.04$, equal to the content of Figs. 1 and 2 of the main text. (a) Normal (particle $G_q = \mathcal{G}_q^{\uparrow\uparrow}$, hole $\bar{G}_q = \mathcal{G}_q^{\downarrow\downarrow}$) and anomalous ($F_q = \mathcal{G}_q^{\uparrow\downarrow}$) components of the local Nambu-Gor'kov Green function $\mathcal{G}_q^{\text{loc}} = \sum_{\mathbf{k}} \mathcal{G}_q(\mathbf{k})$ for different values of q at fixed $T/W = 6.7 \times 10^{-3}$. The OP is taken at $\tau = 0^+$ which we indicate by an arrow. (b) Momentum dependence of the OP normalized to the $q = 0$ value for various T values. The condition $|\Psi_q/\Psi_0| = 1/\sqrt{2}$ to determine the correlation length via $\xi = 1/(\sqrt{2}Q)$ is drawn with dashed lines. Different temperatures T are indicated in the color bar by white triangular markers and the shaded areas for each T show the range spanned by the uncertainty $\delta|\Psi_q|$ which we use for spline fitting to determine an error for ξ . (c) Temperature dependence of ξ as obtained from panel (b) with the same coloring for each temperature. The fit of Eq. (S3) (Eq. (2) in the main text) to extract ξ_0 is plotted with a solid black line.

In Fig. S3, we show the normal (G , \bar{G}) and anomalous (F) Green functions on imaginary time for different values of $q = |q|$ where we also indicate the point of taking $|\Psi_q|$ at $\tau = 0^+$. The amplitude of F is reduced by increasing q , whereas G and \bar{G} change only slightly. Interestingly, the anomalous Green function is a non-monotonous function of τ .

In the main text, we discuss the momentum-dependence of the OP obtained in DMFT calculations under the constraint of FMP. Here, we want to further elaborate on how ξ is obtained from Ψ_q . In GL theory, we found that $\xi = q_c^{-1}$ for $\Psi_{q_c} = 0$. Since the point where Ψ_q goes to zero is difficult to evaluate numerically, we use in our DMFT calculations the criterion $|\Psi_q/\Psi_0| = 1/\sqrt{2}$ deriving from Eq. (S5) such that $\xi = 1/(\sqrt{2}|Q|)$. In Fig. S3(b), we illustrate how this criterion is applied to the DMFT results. Since our microscopic calculations include higher order terms of the free energy, the exact momentum dependence of Ψ_q differs from the GL expectation (Eq. (S5)). Note that we take ξ to be isotropic due to the high symmetry of the fcc lattice. In principle, it is possible to apply FMP with q in different directions in order to consider anisotropic behavior of ξ .

Fig. 2 in the main text and Fig. S3 here in the Supplemental Material show error bars for ξ which result from propagating the statistical QMC error of the OP to ξ . The uncertainty in ξ has been estimated as follows: For every dataset $|\Psi_q(T)|$ we perform a series of spline fits where we randomly vary for each q the values to be fit in the range of $[|\Psi_q| - \delta|\Psi_q|, |\Psi_q| + \delta|\Psi_q|]$ spanned by the uncertainty $\delta|\Psi_q|$ of the OP. We indicate this range by color-shaded areas in Fig. S3(b). Based on each spline interpolation, we obtain a value for Q . The error in Q is then estimated as the standard deviation of Q values in the so-obtained ensemble.

The temperature dependence of extracted ξ and their uncertainty is plotted in panel (c) of Fig. S3. As expected from GL theory, the coherence length diverges towards the critical temperature T_c and decays to a finite value ξ_0 for $T \rightarrow 0$. By fitting Eq. (S3) to the data, we can extract the coherence length ξ_0 and also obtain a value for the critical temperature T_c . We discuss the importance of extracting T_c this way in Sec. S5C.

B. Current density and penetration depth

We derived in Sec. S4C an expression for the current density j_q where we in practice employ the modified Eq. (S42) to ensure better convergence of the Matsubara summations. We show results of $j_q = |j_q|$ depending on the interaction value U/W for the *ab initio* estimated Hund's coupling value $J/W = -0.04$ and fixed $T/W = 6.7 \times 10^{-2}$ in Fig. S4(a). j_q exhibits a maximum, the depairing current j_{dp} , that we obtain by using a spline interpolation of the calculated

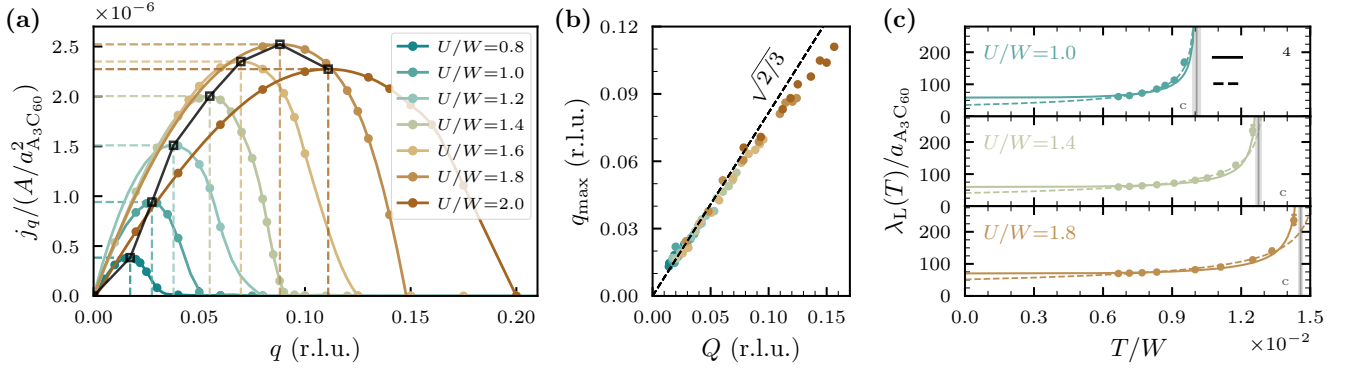


Figure S4. Evaluation of supercurrent density $j_q = |j_q|$ and London penetration depth λ_L . (a) Momentum-dependence of the current density for different interaction ratios U/W with $J/W = -0.04$ similar to Fig. 2 of the main text and fixed $T/W = 6.7 \times 10^{-2}$. The depairing current density j_{dp} (maximal j_q) and corresponding momentum q_{max} are marked by dotted lines which are extracted from a spline interpolation drawn with a solid line connecting data points. The dome-shape behavior of j_{dp} as a function of U/W is marked by a black solid line. (b) Correlation between the momentum Q used to calculate ξ from the suppression of the OP (c.f. Sec. S5 A) and the momentum q_{max} of maximal current density j_{dp} . Data points of the same color correspond to different temperatures for the same U/W where the coloring is the same as in panel (a). A linear function with slope $\sqrt{2/3}$ indicated by a dashed black line fits the data well. (c) Temperature dependence of the London penetration depth λ_L for different U/W and $J/W = -0.04$. We plot the fit according to Eq. (S11) (Eq. (3) in the main text) with the quartic temperature dependence with a solid line and the fit with a linear temperature dependence with a dashed line ($t = T/T_c$).

data. By increasing U/W , j_{dp} exhibits a dome shape which is similar to the OP but different to T_c . We note that the momenta q_{max} where $j_{dp} = j_{q_{max}}$ correlate with the momenta Q used to calculate ξ from the OP suppression as can be seen in panel (b). A line of slope $\sqrt{2/3}$ fits the data well suggesting $q_{max} = \sqrt{2/3}Q$ as expected from the GL description. Only for large U , i.e., large values of Q and q_{max} , small deviations can be seen which arise from the fact that our DMFT calculations include higher order terms which are not accounted for in the GL expansion in Eq. (S4).

From combining the depairing current and the coherence length, we obtain the London penetration depth $\lambda_L(T)$. In GL theory, the T -dependence of λ_L is linearized to depend on $t = T/T_c$. However, our calculations are better described by using the empirical quartic power law t^4 as stated in Eq. (S11) (Eq. (3) of the main text). We show exemplary results for different U/W and $J/W = -0.04$ in Fig. S4(c). At small U , the t and t^4 dependence both match the data points quite well but the t -fit yields smaller values for the zero-temperature limit $\lambda_{L,0}$. Close to the Mott state for large U , the agreement becomes worse and only the t^4 dependence fits the data well. We observed this behavior also for increased values of $|J|$.

C. Proximity region to Mott transition

From our analysis of the T -dependence of the zero-momentum OP $|\Psi_0|$, coherence length ξ , and London penetration depth λ_L , we are able to obtain different values of the superconducting transition temperature T_c . In this section, we discuss how they compare and use the notation of $T_c^{\xi, \lambda}$ to differentiate the critical temperatures obtained by fitting $\xi(T)$ and $\lambda_L(T)$ from the T_c derived via $|\Psi_0|^2 \sim T - T_c$.

A first understanding can be gained by analyzing Fig. 2 of the main text. We summarize the respective critical temperatures in Fig. S5(a). Generally, the critical temperature values obtained in all three methods agree well. Only in the special case of the first-order transition from the superconducting to the Mott-insulating phase for $U/W = 2$, we obtain higher values for $T_c^{\xi, \lambda}$. We conjecture that these temperatures describe a second-order transition to a metallic state hidden by the Mott insulating phase. We can utilize this fact to gauge the influence of the Mott state to reveal a suppression of superconductivity.

In Fig. S5(b), we show the critical temperature T_c and the relative difference to $T_c^{\xi, \lambda}$ in the (U, J) -plane analogous to Fig. 3 of the main text. Dots indicate original data points where orange dots (not shown in Fig. 3) denote a critical temperature for a first-order transition from superconductor to Mott insulator. At these points, both T_c^{ξ} and T_c^{λ} are

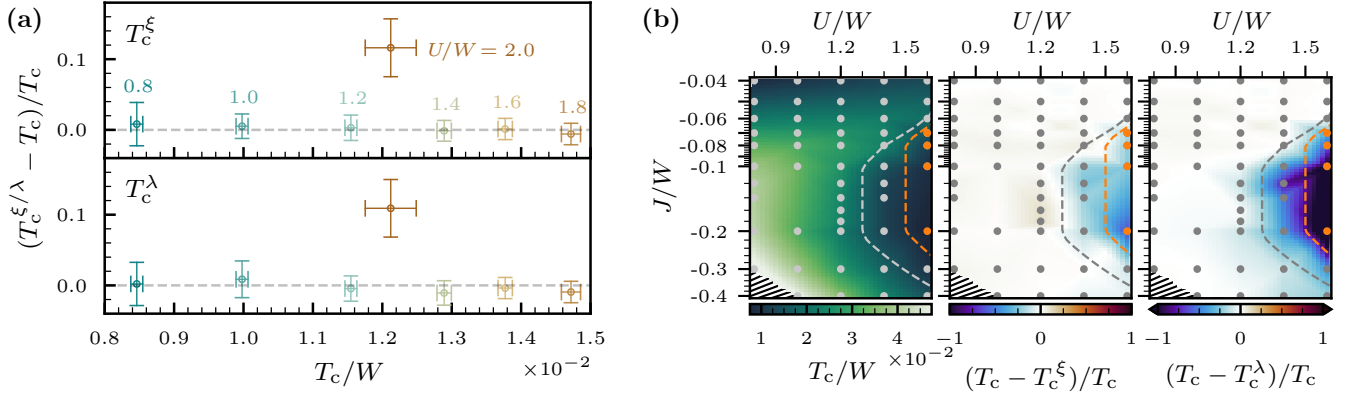


Figure S5. Influence of proximity to the Mott insulating region on the superconducting state. (a) Relative difference of critical temperature $T_c^{(\xi, \lambda)}$ computed from fitting $\xi(T)$ and $\lambda_L(T)$ versus T_c as obtained from the OP $|\Psi_0|$ for the data at $J/W = -0.04$ and different U/W as plotted in Fig. 2 of the main text. (b) T_c and relative difference to $T_c^{(\xi, \lambda)}$ as a function of interactions U and J . Orange (gray) dots indicate data points where the critical temperature describes a transition from superconducting to Mott insulating (metallic) phase. Dashed lines are a guide to the eye separating the regions where the proximity to the Mott phase suppresses superconductivity characterized by $T_c^{(\xi, \lambda)} < T_c$. The T_c plot is the same as in Fig. 3 of the main text.

clearly larger than the critical temperature obtained from $|\Psi_0|^2$ which is inline with the observation at $J/W = -0.04$. However, the suppression of T_c extends to the nearby region of the direct superconductor-Mott transition. The dashed lines, which we also draw in Fig. 3 of the main text, are a guide to the eye to separate the region where proximity to Mott insulating states leads to a suppression of the critical temperature – even for a transition to the metallic state.

S6. ATOMIC LIMIT OF THREE-ORBITAL MODEL WITH INVERTED HUND'S COUPLING

In the main text, we found that Cooper pairs become very localized with a short coherence length $\xi_0 \sim \mathcal{O}(2 - 3 a_{\text{A}_3\text{C}_{60}})$ by increasing the inverted Hund's coupling $J < 0$. It suggests that local physics become increasingly important for the formation of superconducting pairing. Indeed, this was confirmed through the analysis of local density matrix weights in the main text. Here, we want to complement the discussion of the main text with discussing the atomic limit of the interacting impurity problem.

To this end, we want to solve the Kanamori-Hubbard interaction Hamiltonian as given in Eq. (7) of the main text without hopping processes. The form of the interaction given in the main text is convenient to read-off the (inverted) Hund's rules. We, here, restate the Kanamori-Hubbard Hamiltonian in its generalized formulation that indicates the different electronic interaction processes more clearly:

$$H_{\text{int}} = \sum_{\alpha} U n_{\alpha\uparrow} n_{\alpha\downarrow} + \sum_{\alpha < \gamma, \sigma\sigma'} (U' - \delta_{\sigma\sigma'} J) n_{\alpha\sigma} n_{\gamma\sigma'} - \sum_{\alpha \neq \gamma} J_X c_{\alpha\uparrow}^{\dagger} c_{\alpha\downarrow} c_{\gamma\downarrow}^{\dagger} c_{\gamma\uparrow} + \sum_{\alpha \neq \gamma} J_P c_{\alpha\uparrow}^{\dagger} c_{\alpha\downarrow}^{\dagger} c_{\gamma\downarrow} c_{\gamma\uparrow}. \quad (\text{S52})$$

It consists of intraorbital interaction U , interorbital interaction U' , Hund's coupling J , spin-exchange J_X , and correlated pair hopping J_P . Yet, not all coupling constants are independent. We assume $\text{SU}(2) \times \text{SO}(3)$ symmetry implying $J_X = J$ and $J_P = U - U' - J$ [S31]. In the physical system and our calculations, we have in addition $J_P = J$ resulting in $U' = U - 2J$. In the following discussion, we will, however, focus the contribution of J_P since the low-energy excitations for inverted Hund's coupling $J < 0$ are only governed by J_P . It is instructive to rewrite Eq. (S52) in the same way as Eq. (7) of the main text to see the role of J_P :

$$H_{\text{int}} = \frac{1}{4}(2U - 3J - 3J_P)\hat{N}(\hat{N} - 1) - (J + J_P)\hat{S}^2 + \frac{1}{2}J_P\hat{L}^2 - \frac{1}{4}(3J + 7J_P)\hat{N}. \quad (\text{S53})$$

The pair hopping term, most notably, dictates the energy gain from the orbital angular momentum L^2 and partially that of the total spin S^2 of a given eigenstate for this Hamiltonian. We detail the spectrum in Table S1 for the case

of negative J , $J_P < 0$ and half-filled orbitals where we add a chemical potential μ to ensure particle-hole symmetry.⁷ The dimension of the complete Fock space is $\dim \mathcal{H}_{\text{Fock}} = 2^6 = 64$.

The atomic gap of the system is $\Delta_{\text{at}} = E_0^{N=4} - E_0^{N=3} - (E_0^{N=3} - E_0^{N=2}) = U + 2J_P = U - 2|J_P|$. For the case of $\Delta_{\text{at}} > 0$, i.e., $U > 2|J_P|$, the lowest energy state lies in the $N = 3$ particle sector and is given by $E_0^{N=3}$. We sketch the energy spectrum for this case in Fig. S6. The lowest energy excitations from this state are charge excitation from $N = 3$ to the $N = 2$ and $N = 4$ particle sectors with $\Delta E_{\text{ch}} = \frac{1}{2}U + J_P = \frac{1}{2}U - |J_P| \equiv \frac{1}{2}\Delta_{\text{at}}$ as well as spin reconfiguration with $\Delta E_{\text{sp}} = -2J_P = 2|J_P|$ in the $N = 3$ charge sector which increases the orbital angular momentum from $L = 1$ to $L = 2$. Thus, the low-energy physics is governed by correlated pair hopping J_P and onsite repulsion U .

Table S1. Spectrum of the local Kanamori-Hubbard Hamiltonian (Eq. (S53)) for a three-orbital system at half-filling. The eigenenergies E_n^N are sorted in descending order in each charge sector of particle number N for $J < 0$ where the contribution of the correlated pair hopping J_P ($J_P \equiv J$ in our calculations) is explicitly stated. Each state is characterized by their total spin S , orbital angular momentum L , and respective degeneracy $(2S+1)(2L+1)$ with $X = \langle \hat{X} \rangle$ ($X = N, S, L$). The corresponding eigenstates $|\phi_n^N\rangle$ are given for $N \leq 3$ since the $N \geq 4$ states can be constructed from particle-hole symmetry. The eigenstates in blue color are those depicted in Fig. 3(d) of the main text.

Energy E_n^N	N	S	L	Degeneracy ($2S+1$)($2L+1$)	Eigenstates $ \phi_n^N\rangle$ ($N \leq 3$)
$E_0^{[6]} = 0$	0 [6]	0	0	1	$ 0, 0, 0\rangle$
$E_0^{[5]} = -\frac{5}{2}U + 3J + 2J_P$	1 [5]	1/2	1	6	$ \uparrow, 0, 0\rangle, 0, \uparrow, 0\rangle, 0, 0, \uparrow\rangle,$ $ \downarrow, 0, 0\rangle, 0, \downarrow, 0\rangle, 0, 0, \downarrow\rangle$
$E_2^{[4]} = -4U + 4J + 3J_P$	2 [4]	1	1	9	$ \uparrow, \uparrow, 0\rangle, 0, \uparrow, \uparrow\rangle, \uparrow, 0, \uparrow\rangle, \downarrow, 0, \downarrow\rangle, 0, \downarrow, \downarrow\rangle, \downarrow, 0, \uparrow\rangle,$ $\frac{1}{\sqrt{2}}(\uparrow, 0, \downarrow\rangle - \downarrow, 0, \uparrow\rangle), \frac{1}{\sqrt{2}}(0, \uparrow, \downarrow\rangle - 0, \downarrow, \uparrow\rangle), \frac{1}{\sqrt{2}}(\uparrow, \downarrow, 0\rangle - \downarrow, \uparrow, 0\rangle)$
$E_1^{[4]} = -4U + 6J + 3J_P$	2 [4]	0	2	5	$\frac{1}{\sqrt{2}}(\uparrow, 0, \downarrow\rangle + \downarrow, 0, \uparrow\rangle), \frac{1}{\sqrt{2}}(0, \uparrow, \downarrow\rangle + 0, \downarrow, \uparrow\rangle), \frac{1}{\sqrt{2}}(\uparrow, \downarrow, 0\rangle + \downarrow, \uparrow, 0\rangle)$ $\frac{1}{\sqrt{2}}(\uparrow\downarrow, 0, 0\rangle - 0, \uparrow\downarrow, 0\rangle), \frac{1}{\sqrt{2}}(\uparrow\downarrow, 0, 0\rangle - 0, 0, \uparrow\downarrow\rangle)$
$E_0^{[4]} = -4U + 6J + 6J_P$	2 [4]	0	0	1	$\frac{1}{\sqrt{3}}(\uparrow\downarrow, 0, 0\rangle + 0, \uparrow\downarrow, 0\rangle + 0, 0, \uparrow\downarrow\rangle)$
$E_2^3 = -\frac{9}{2}U + 3J + 3J_P$	3	3/2	0	4	$ \uparrow, \uparrow, \uparrow\rangle, \frac{1}{\sqrt{3}}(\uparrow, \downarrow, \downarrow\rangle + \downarrow, \uparrow, \downarrow\rangle + \downarrow, \downarrow, \uparrow\rangle),$ $ \downarrow, \downarrow, \downarrow\rangle, \frac{1}{\sqrt{3}}(\downarrow, \uparrow, \uparrow\rangle + \uparrow, \downarrow, \uparrow\rangle + \uparrow, \uparrow, \downarrow\rangle)$
$E_1^3 = -\frac{9}{2}U + 6J + 3J_P$	3	1/2	2	10	$\frac{1}{\sqrt{2}}(\uparrow, \uparrow, \downarrow\rangle - \downarrow, \uparrow, \downarrow\rangle), \frac{1}{\sqrt{2}}(\uparrow, \downarrow, \downarrow\rangle - \downarrow, \downarrow, \uparrow\rangle),$ $\frac{1}{\sqrt{2}}(\uparrow, \uparrow\downarrow, 0\rangle - \uparrow, 0, \uparrow\downarrow\rangle), \frac{1}{\sqrt{2}}(\uparrow\downarrow, \uparrow, 0\rangle - 0, \uparrow\downarrow\rangle), \frac{1}{\sqrt{2}}(\uparrow\downarrow, 0, \uparrow\rangle - 0, \uparrow\downarrow, \uparrow\rangle),$ $\frac{1}{\sqrt{2}}(\downarrow, \uparrow\downarrow, 0\rangle - \downarrow, 0, \uparrow\downarrow\rangle), \frac{1}{\sqrt{2}}(\uparrow\downarrow, \downarrow, 0\rangle - 0, \downarrow, \uparrow\downarrow\rangle), \frac{1}{\sqrt{2}}(\uparrow\downarrow, 0, \downarrow\rangle - 0, \uparrow\downarrow, \downarrow\rangle),$ $\frac{1}{\sqrt{2}}(\downarrow, \uparrow, \uparrow\rangle - \uparrow, \downarrow, \uparrow\rangle), \frac{1}{\sqrt{2}}(\downarrow, \uparrow, \uparrow\rangle - \uparrow, \uparrow, \downarrow\rangle)$
$E_0^3 = -\frac{9}{2}U + 6J + 5J_P$	3	1/2	1	6	$\frac{1}{\sqrt{2}}(\uparrow, \uparrow\downarrow, 0\rangle + \uparrow, 0, \uparrow\downarrow\rangle), \frac{1}{\sqrt{2}}(\uparrow\downarrow, \uparrow, 0\rangle + 0, \uparrow, \uparrow\downarrow\rangle), \frac{1}{\sqrt{2}}(\uparrow\downarrow, 0, \uparrow\rangle + 0, \uparrow\downarrow, \uparrow\rangle),$ $\frac{1}{\sqrt{2}}(\downarrow, \uparrow\downarrow, 0\rangle + \downarrow, 0, \uparrow\downarrow\rangle), \frac{1}{\sqrt{2}}(\uparrow\downarrow, \downarrow, 0\rangle + 0, \downarrow, \uparrow\downarrow\rangle), \frac{1}{\sqrt{2}}(\uparrow\downarrow, 0, \downarrow\rangle + 0, \uparrow\downarrow, \downarrow\rangle)$

⁷ The chemical potential at half-filling is given by $\mu = \frac{1}{2}U + \frac{N-1}{2}(2U' - J) = \frac{5}{2}U - 3J - 2J_P$ with $N = 3$ and $U' = U - J - J_P$, as can be inferred from particle-hole transforming Eq. (S53).

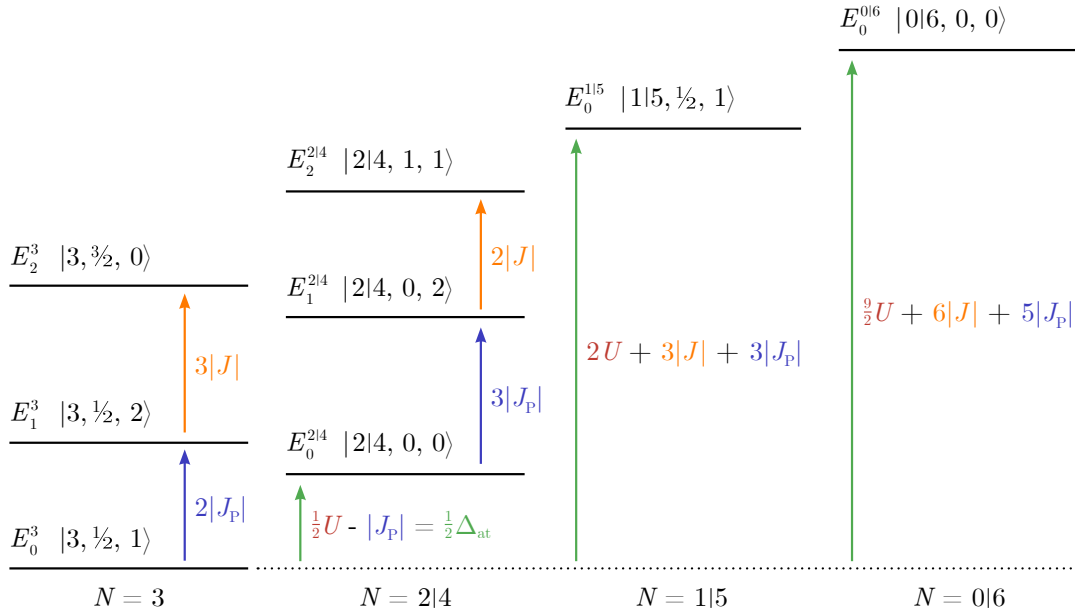


Figure S6. Visualization of the spectrum in Tab. S1 for the three-orbital atom with Hubbard-Kanamori interaction (Eq. (S53)) at half-filling with energy E_n^N and state $|\phi_n^N\rangle \equiv |N, S, L\rangle$. The relative positions of energies are drawn for the case of $U > 2|J_P|$, such that the ground state lies in the $N=3$ sector given by E_0^3 and $|N=3, S=\frac{1}{2}, L=1\rangle$.

-
- [S1] N. F. Q. Yuan and L. Fu, Supercurrent diode effect and finite-momentum superconductors, *Proceedings of the National Academy of Sciences* **119**, 10.1073/pnas.2119548119 (2022).
- [S2] P. Fulde and R. A. Ferrell, Superconductivity in a Strong Spin-Exchange Field, *Physical Review* **135**, A550 (1964).
- [S3] A. I. Larkin and Y. N. Ovchinnikov, Nonuniform state of superconductors, *Zh. Eksp. Teor. Fiz.* **47**, 1136 (1964).
- [S4] J. J. Kinnunen, J. E. Baarsma, J.-P. Martikainen, and P. Törmä, The Fulde-Ferrell-Larkin-Ovchinnikov state for ultra-cold fermions in lattice and harmonic potentials: a review, *Reports on Progress in Physics* **81**, 046401 (2018).
- [S5] D. F. Agterberg, J. S. Davis, S. D. Edkins, E. Fradkin, D. J. V. Harlingen, S. A. Kivelson, P. A. Lee, L. Radzihovsky, J. M. Tranquada, and Y. Wang, The Physics of Pair-Density Waves: Cuprate Superconductors and Beyond, *Annual Review of Condensed Matter Physics* **11**, 231 (2020).
- [S6] P. Coleman, *Introduction to Many-Body Physics* (Cambridge University Press, 2008).
- [S7] R. Shimano and N. Tsuji, Higgs Mode in Superconductors, *Annual Review of Condensed Matter Physics* **11**, 103 (2020).
- [S8] J. Bardeen, Theory of Superconductivity, in *Encyclopedia of Physics / Handbuch der Physik* (Springer Berlin Heidelberg, 1956) pp. 612–707.
- [S9] J. Bardeen, L. N. Cooper, and J. R. Schrieffer, Theory of Superconductivity, *Physical Review* **108**, 1175 (1957).
- [S10] I. Khalatnikov and A. Abrikosov, The modern theory of superconductivity, *Advances in Physics* **8**, 45 (1959).
- [S11] M. Tinkham, *Introduction to superconductivity*, 2nd ed. (Dover Publications, 2004) p. 454.
- [S12] D. Pekker and C. Varma, Amplitude/Higgs Modes in Condensed Matter Physics, *Annual Review of Condensed Matter Physics* **6**, 269 (2015).
- [S13] D.-H. Kim, J. J. Kinnunen, J.-P. Martikainen, and P. Törmä, Exotic Superfluid States of Lattice Fermions in Elongated Traps, *Physical Review Letters* **106**, 095301 (2011).
- [S14] D.-H. Kim and P. Törmä, Fulde-Ferrell-Larkin-Ovchinnikov state in the dimensional crossover between one- and three-dimensional lattices, *Physical Review B* **85**, 180508 (2012).
- [S15] M. O. J. Heikkinen, D.-H. Kim, and P. Törmä, Finite-temperature stability and dimensional crossover of exotic superfluidity in lattices, *Physical Review B* **87**, 224513 (2013).
- [S16] M. Heikkinen, D.-H. Kim, M. Troyer, and P. Törmä, Nonlocal Quantum Fluctuations and Fermionic Superfluidity in the Imbalanced Attractive Hubbard Model, *Physical Review Letters* **113**, 185301 (2014).
- [S17] K.-E. Huhtinen, M. Tylutki, P. Kumar, T. I. Vanhala, S. Peotta, and P. Törmä, Spin-imbalanced pairing and Fermi surface deformation in flat bands, *Physical Review B* **97**, 214503 (2018).
- [S18] Y. Nomura, K. Nakamura, and R. Arita, Ab initio derivation of electronic low-energy models for C₆₀ and aromatic

- compounds, [Physical Review B](#) **85**, 155452 (2012).
- [S19] A. Georges, G. Kotliar, and W. Krauth, Superconductivity in the two-band hubbard model in infinite dimensions, [Zeitschrift für Physik B Condensed Matter](#) **92**, 313 (1993).
- [S20] A. Georges, G. Kotliar, W. Krauth, and M. J. Rozenberg, Dynamical mean-field theory of strongly correlated fermion systems and the limit of infinite dimensions, [Reviews of Modern Physics](#) **68**, 13 (1996).
- [S21] A. A. Abrikosov, L. P. Gorkov, and I. E. Dzyaloshinski, *Methods of quantum field theory in statistical physics* (Dover Publications, 1975) p. 352.
- [S22] E. Gull, A. J. Millis, A. I. Lichtenstein, A. N. Rubtsov, M. Troyer, and P. Werner, Continuous-time Monte Carlo methods for quantum impurity models, [Reviews of Modern Physics](#) **83**, 349 (2011).
- [S23] P. Werner, A. Comanac, L. de' Medici, M. Troyer, and A. J. Millis, Continuous-Time Solver for Quantum Impurity Models, [Physical Review Letters](#) **97**, 076405 (2006).
- [S24] Y. Nomura, S. Sakai, M. Capone, and R. Arita, Unified understanding of superconductivity and Mott transition in alkali-doped fullerides from first principles, *Science Advances* **1**, [10.1126/sciadv.1500568](#) (2015).
- [S25] Y. Nomura, S. Sakai, M. Capone, and R. Arita, Exotic *s*-wave superconductivity in alkali-doped fullerides, [Journal of Physics: Condensed Matter](#) **28**, 153001 (2016).
- [S26] S. Hoshino and P. Werner, Spontaneous Orbital-Selective Mott Transitions and the Jahn-Teller Metal of A_3C_{60} , [Physical Review Letters](#) **118**, 177002 (2017).
- [S27] D. J. Scalapino, J. R. Schrieffer, and J. W. Wilkins, Strong-Coupling Superconductivity. I, [Physical Review](#) **148**, 263 (1966).
- [S28] T. Takimoto and T. Moriya, Theory of Spin Fluctuation-Induced Superconductivity Based on a *d-p*-Model. II. - Superconducting State-, [Journal of the Physical Society of Japan](#) **67**, 3570 (1998).
- [S29] E. Gull and A. J. Millis, Pairing glue in the two-dimensional hubbard model, [Physical Review B](#) **90**, 041110 (2014).
- [S30] X. Dong, E. Gull, and A. J. Millis, Quantifying the role of antiferromagnetic fluctuations in the superconductivity of the doped Hubbard model, [Nature Physics](#) **18**, 1293 (2022).
- [S31] A. Georges, L. de' Medici, and J. Mravlje, Strong Correlations from Hund's Coupling, [Annual Review of Condensed Matter Physics](#) **4**, 137 (2013).